Universidade de Aveiro
2017

Departamento de Química

Luís Miguel Marques Barbosa

Produção e caracterização da fusão ZZapo-CBM$_{64}$ para captura e deteção da apolipoproteína-A1 em testes de papel

Production and characterization of the fusion ZZapo-CBM$_{64}$ for the capture and detection of apolipoprotein-A1 in paper tests

Dissertação apresentada à Universidade de Aveiro para cumprimento dos requisitos necessários à obtenção do grau de Mestre em Bioquímica, ramo de Métodos Biomoleculares, realizada sob a orientação científica do Professor Duarte Miguel Prazeres, Professor Catedrático do Instituto Superior Técnico de Lisboa, e da Professora Maria do Rosário Domingues, Professora Associada com Agregação do Departamento de Química da Universidade de Aveiro

Apoio financeiro da FCT, da União Europeia, QREN, no âmbito do Programa Operacional Temático Fatores de Competitividade (COMPETE).

Apoio financeiro à unidade de investigação QOPNA (projeto PEst-C/QUI/UI0062/2013; FCOMP-01-0124-FEDER-037296) e RNEM.

o júri

Presidente — Prof. Doutor Francisco Manuel Lemos Amado

Professor Associado com Agregação no Departamento de Química da Universidade de Aveiro

Arguente — Prof. Doutora Rita Maria Pinho Ferreira

Professora Auxiliar no Departamento de Química da Universidade de Aveiro

Vogal — Prof. Doutor Duarte Miguel de França Teixeira dos Prazeres

Professor Catedrático do Instituto Superior Técnico de Lisboa

Agradecimentos A realização desta dissertação contou com importantes apoios sem os quais não teria sido possível completar esta etapa. Em primeiro e mais importante, aos meus pais, que me apoiaram durante toda a minha vida académica, ao incentivo e à paciência que apresentaram mesmo quando se apresentaram obstáculos.

Um grande obrigado ao Prof. Doutor Miguel Prazeres por toda a ajuda dada e pela oportunidade de poder desenvolver este trabalho no seu grupo de investigação, onde pude desenvolver ainda mais os meus conhecimentos.

Outro agradecimento à Prof. Rosário Domingues Pelo acompanhamento e pela orientação deste trabalho.

Por último, também dedico este espaço para agradecer a todos os meus amigos e colegas que me deram um grande apoio, tanto a nível de trabalho, como emocional, Sónia Ruivo, Ana Rosa, Rui Silva, Flávio Ferreira, Augusto Souto, Eduarda Morais, Joana Pereira e todos os restantes que me acompanharam nesta fase.

Palavras-chave Microfluídica, Aparelhos Microfluídicos de Papel, Nanopartículas de Ouro, Affibodies, Imunodeteção, Impressão de cera, ELISA, Anticorpos, Apolipoproteína-A1, Ensaios Lateral Flow

Resumo Affibodies (ZZ) são pequenas proteínas de afinidade que podem ser modificadas para se ligarem a alvos específicos. Estas proteínas têm sido sugeridas como uma alternativa a anticorpos, devido ao seu processo de produção mais simples e barato. Assim, o objetivo deste trabalho de mestrado visou a possibilidade da utilização de um affibody (ZZapo) para a captura da Apolipoproteina-A1 (Apo-A1) e sua deteção com anticorpos Anti-Apo-A1 conjugados com Nanopartículas de Ouro (AuNPs) num Dispositivo Microfluídico Analítico de Papel (µPAD). Para atingir o objetivo proposto, a fusão de uma molécula com afinidade a carboidratos da família 64 (CBM_{64}) com o affibody ZZapo (ZZapo-CBM_{64}) foi desenhada, produzida em *E.coli*, sequenciada, purificada e quantificada com sucesso. A fusão ZZapo-CBM_{64} foi comparada com a fusão semelhante ZZ-CBM_{64}, que tem afinidade para imunoglobulina G (IgG). Foi testada a capacidade de ligação das fusões à celulose, tendo-se verificado que ambas apresentaram alta afinidade a micropartículas e papel de celulose. Foi ainda testada a capacidade de ligação das duas fusões a IgG, pela utilização de IgG marcado com fluorescência. No entanto, ao contrário da ZZ-CBM_{64}, a ZZapo-CBM_{64} não mostrou afinidade para a IgG. Um teste µPAD foi criado com barreiras impressas a cera hidrofóbica, e com um adesivo na base do teste, o que permitiu os testes serem feitos em superfícies planas e ainda contribuiu para um fluxo da amostra mais rápido. Os testes µPAD mostraram interações não específicas entre ZZapo-CBM_{64} e AuNPs, que foram removidas pela conjugação das AuNPs com Albumina de Soro Bovino (BSA) e adição de BSA e Tween20 à solução tampão. Os testes µPAD para deteção da Apo-A1 mostraram interações não específicas entre Apo-A1 e a membrana adesiva, que foram removidas pela utilização de um tampão de Bicarbonato de Amónia com BSA e Tween20. A deteção de Apo-A1 em µPADs não foi conseguida devido ao ZZapo-CBM_{64} não capturar a Apo-A1. Esta falha poderá ser devido a algum bloqueio da zona de captura relacionado com a estrutura 3D da fusão. De modo a ultrapassar esta questão, deverão ser realizados trabalhos futuros para o estudo da estrutura 3D da fusão, assim como estudo de outras fusões com diferentes variantes de affibodies para averiguar se o problema é exclusivo à fusão ZZapo-CBM_{64} ou não.

Keywords Affibodies, Microfluidics, Paper-based microfluidic devices, Gold Nanoparticles, Immunoassays, Wax Printing, ELISA, Antibodies, Apolipoprotein-A1, Lateral Flow Assays

Abstract Affibodies (ZZ) are small affinity proteins that can be engineered to bind to specific targets. These molecules have emerged as an alternative to antibodies due to their simpler and cheaper production process. The objective of this work was thus to assess the possibility of using an affibody (ZZapo) to capture Apolipoprotein-A1 (Apo-A1) and its detection using Anti-Apo-A1 antibodies conjugated to Gold Nanoparticles (AuNPs) on a Microfluidic Paper-Based Analytical Device (µPAD). To achieve the proposed objective, a fusion of a Carbohydrate Binding Molecule of the family 64 (CBM_{64}) with a ZZapo affibody (ZZapo-CBM_{64}) was successfully designed, produced in *E. coli*, sequenced, purified and quantified. The ZZapo-CBM_{64} fusion was then compared to a similar ZZ-CBM_{64} fusion (produced and purified in the same way) with immunoglobulin G (IgG) binding capacity, and tested for its cellulose binding capacity. Both fusions showed high affinity to cellulose particles and paper. They were also tested for IgG binding capacity, using a fluorescently labelled IgG. While ZZ-CBM_{64} successfully captured IgG, the new ZZapo-CBM_{64} did not capture the labelled IgG. A µPAD test was designed and produced with wax printed hydrophobic barriers, and the use of an adhesive membrane in the bottom of the test enabled running tests on a flat surface, and contributed for faster sample flow. µPAD tests showed that ZZapo-CBM_{64} and AuNPs had non-specific interactions, which were removed by conjugating AuNPs with Bovine Serum Albumin (BSA) and using a buffer containing BSA and Tween20. µPAD tests for the detection of Apo-A1 showed non-specific binding of Apo-A1 and the adhesive membrane, which was removed by using ammonium bicarbonate buffer. Apo-A1 detection in µPADs was unsuccessful, which was shown to be caused by ZZapo-CBM_{64} failing to capture Apo-A1. This failed capture could be caused by the capture zone of the protein being blocked. Future works should be directed to the study of the 3D structure of this fusion, as well as the study of other fusions with different affibody variants to assess if this problem is exclusive to ZZapo-CBM_{64} or not.

TABLE OF CONTENTS

LIST OF FIGURES

LIST OF TABLES

ABREVIATIONS

3D	*Three-Dimensional*
ABD	*Albumin Binding Domain*
AuNP	*Colloidal Gold Nanoparticle*
AKD	*Alkyl Ketene Dimer*
Apo-A1	*Apolipoprotein-A1*
BCA	*Bicinchoninic Acid*
bp	*Base Pairs*
BSA	*Bovine Serum Albumin*
CBM	*Carbohydrate-Binding Molecule*
DNA	*Deoxyribonucleic Acid*
DTT	*Dithiotheritol*
EDTA	*Ethylenediaminetetraacetic Acid*
EGFR	*Epidermal Growth Factor Receptor*
ELISA	*Enzyme-Linked Immunosorbent Assay*
ePAD	*Electrochemical Paper-Based Analytical Device*
FDA	*Federal Drug Administration*
FITC	*Fluorescein Isothiocyanate*
HAIA	*Heterophilic Anti-Animal Immunoglobulin Antibody*
hCG	*Human Chorionic Gonadotropin*
HDL	*High Density Lipoprotein*
HEPES	*4-(2-Hydroxyethyl)-1-Piperazineethanesulfonic Acid*
HER	*Human Epidermal Growth Factor Receptor*
HSA	*Human Serum Albumin*
IgG	*Immunoglobulin G*
IPTG	*Isopropyl β-D-1-thiogalactopyranoside*
LB	*Luria-Bertani*
LFA	*Lateral Flow Assay*
LSPR	*Locallized Surface Plasmon Resonance*
µPAD	*Microfluidic Paper-Based Analytical Device*

PBS	*Phosphate Buffered Saline*
PDMS	*Poly(dimethylsiloxane)*
PET	*Position Emission Tomography*
PMMA	*Poly(methylmethacryalate)*
PNIPAM	*Poly(N-isopropylacrylamide)*
POC	*Point-of-Care*
RT	*Room Temperature*
SPECT	*Single-Photon Emission Computed Tomography*
ZZ	*Z-Domain Affibody*
ZZapo	*Apolipoprotein-A1 binding Affibody*

INTRODUCTION

1 AFFIBODIES

Antibodies are the most successful and widespread affinity protein used in biochemical applications. The preference of these molecules is due to the capacity of being isolated with high affinity and specificity to any given target, as well as being a well-documented technology and being readily available (1). These molecules, however, also present several limitations caused by their molecular structure, such as low heat stability and complex and expensive manufacturing processes. Although they are large molecules, only a small part of them is used for target recognition and the bulk of the antibody structure adds complexity when evaluating the molecules. As such, there has also been a large focus in the investigation of novel affinity molecules with simpler structures and high affinity and specificity, such as affibody molecules (2).

Affibodies are small proteins (6 kDa), that are engineered to bind to specific proteins. Its scaffold structure is an engineered variant of the B domain (Fc-binding portion) of *Staphylococcal* protein A mutated at key positions for increased chemical stability, the Z-domain (ZZ), which has high affinity to immunoglobulin G (IgG). They possess a three alpha-helix structure, containing 58 amino acids (3,4). Affibody production uses synthetic combinatorial libraries generated by randomizing 13 surface amino acids on helices one and two and using phage display technology, which are highly tolerable to random amino acid substitutions. These libraries are displayed on phages, following biopanning against different targets, creating affibody variants that recognize varied targets such as Taq polymerase, human insulin, human serum albumin and human apolipoprotein-A1 (Apo-A1) (2,4,5). This technology allows recombinant production of affibodies in bacteria, such as *E.coli*, making it cheaper and easier to produce than antibodies. Affibodies can also be produced by chemical peptide synthesis, due to their small size and rapid folding properties, making it possible to introduce functional groups of interest, such as reporting agents (6,7). Even with these extra functional groups, affibodies are still considerably smaller than an antibody. In a recent paper, *Lindgren et al.* (8) reported that solid-phase peptide synthesis of affibodies with fluorophores combines high-yield and purity with simple and fast preparation of different variants of affibodies (8,9). These molecules also present several advantages when

compared with antibodies. Because they are composed of alpha-helices, they do not have disulphide bonds, which enables intracellular applications. They also have a spatially well-defined surface area where amino acids can be modified, as explained previously, to create variants of interest, which have been proven useful to target various signal receptors and cancer-related molecules, such as the production of *in vivo* molecular probes (9).

Affibody research has been largely focused on antigens for tumours, specifically with Human Epidermal Growth Factor Receptor 2 (HER2), which is used as an imaging agent in tumour imaging, a technique that is used to precisely localize primary tumours and metastatic lesions in a non-invasive fashion (9). Affibodies show great promise as imaging agents due to their small structure, resulting in rapid biodistribution and extravasation, and are among the most investigated alternative binding proteins in imaging (2). Baum *et al.* (10) created the first affibody to be used in humans, namely for breast cancer imaging using HER2-binding affibodies.. Several authors have shown the use of labelled affibodies with radionuclides as imaging probes for Single-Photon Emission Computed Tomography (SPECT) and Position Emission Tomography (PET), such as ^{99m}Tc (metastable technetium-99), ^{111}In (indium), ^{68}Ga (gallium) and ^{124}I (iodine), finding that affibodies provided high contrast in imaging due to their affinity to HER2 (11–14). More recently, Sexton *et al.* (15) showed that fluorescently labelled HER2-binding affibodies performed better in tumour imaging than antibodies, due to their smaller size. Furthermore, Rosik *et al.* (16) reported that the biodistribution of these molecules could be improved by inserting a triglutamyl spacer after the radiofluorination with ^{18}F-4-Fluorobenzaldehyde. They also noted that one hour after the injection of affibodies, only the kidneys and tumour were highly marked with radioactivity, however, two hours after the injection only the tumour was marked (16). Gao *et al.* (17) further proved that affibodies are good substitutes for antibodies when used as probes for cell and tumour imaging by conjugating maleimide-functionalized nanoparticles with affibodies that target HER2, verifying a strong signal in magnetic resonance imaging from cells that were incubated with the affibody-nanoparticle conjugates. Another study found that these conjugates have better targeting ability than radiolabelled affibodies, and are also better suited for *in-vivo* testing (18). More recently, another study showed the possibility of generating bispecific affibodies, capable of specifically capturing two targets. This experiment consisted in evaluating the effectiveness of bispecific affibodies, which have two binding domains for HER2 and HER3 to target tumours, and a third albumin

binding domain to provide longer *in-vivo* circulatory life. They found that these bispecific affibodies could bind to any of the three targets, and, in addition, showed an anti-proliferative effect due to inhibiting phosphorylation of HER receptors (7). In 2014, these HER2-binding affibodies were used to detect precursors to metastatic cancer, improving utility and cost effectiveness on HER2-targeted therapies (19,20). One of the most successful experiments in HER2-targeted therapies for radioimmunotherapy used radiometals attached to HER2-binding affibodies fused with a small Albumin Binding Domain (ABD). They found that these ABD-fused affibodies had a significant reduction in kidney cells recognition, and delivered isothiocyanate (a cell apoptosis inducer) to the tumour when compared to the non-ABD-fused affibodies, showing a great potential for tumour-targeted drug delivery (21).

Besides imaging and diagnostics, affibody properties also allow them to be applied in several other fields of study, such as therapeutics, protein purification and bioassays, which we will be exploring further. Affibodies have already been shown useful in protein purification through affinity chromatography. By coupling to affibodies to chromatographic resins, affibody targets can be captured when a complex sample is run through a column packed with this affinity resin (22). Affibodies were shown to be an efficient replacement to antibodies in immunoaffinity chromatography due to their high specificity, performance and simple structure. In order to further investigate efficiency, Anderson *et al.* (23) compared purity and yield of a Human Serum Albumin (HSA) Sepharose column with an affibody-targeted column in the separation of G protein from hamster kidney cells, and found that affibodies provided a much higher yield and purity. More recently, these molecules were used in affinity chromatography to recover other affibody variants with common HER2 binding surface, which showed efficient capture with high specificity and sensitivity, thus further supporting the efficiency of affibodies in protein purification (22).

Affibodies have also been applied in protein capture and detection and used as affinity probes in bioassays (20). Recently, anti-IgG affibodies conjugated with polystyrene nanobeads were shown to be more effective in the capacity to immobilize the fluorescently labelled IgG in comparison to microbeads, while also functioning as a sandwich assay to detect the amount of antibody with a very small sample (24). Andersson *et al.* (5) reported the use of affibodies in Enzyme-Linked Immunosorbent Assay (ELISA) as a way to remove false positives caused by Heterophilic Anti-Animal Ig Antibodies (HAIA) present in human serum in “sandwich” assays (Figure 1). HAIA can cross-link with capture and detection

antibodies creating false positives (25). The replacement of a capture or detection antibody with an affibody in these assays was reported to be an efficient way to remove HAIA interferences in ELISA as an alternative to other workarounds involving the use of more antibodies (5).

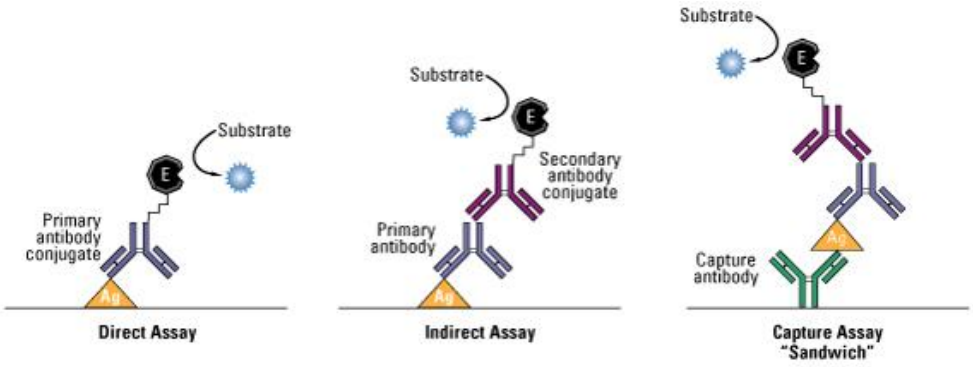

Figure 1 - Common ELISA formats using a primary antibody coupled to an enzyme to yield a coloured product. Direct and indirect assays do not bind the analyte to a capture antibody, whereas capture assays do. Secondary conjugated antibodies are used in indirect assays. Adapted from (26).

These studies show that affibodies are an emerging affinity molecule that could advantageously replace antibodies – they are cheaper and simpler to synthesize, their structure is less complex and can be used wide range of applications, especially in imaging, diagnostics and therapeutics. The incorporation of affibodies in bioassays and biosensors are not as well reported and should be further investigated due to their high specificity and affinity properties. As such, in this study, an affibody with binding affinity to Apo-A1 (ZZapo), previously reported in literature (4), will be studied for its capacity of substituting Apo-A1 capture antibodies in a "sandwich" immunoassay.

2 APOLIPOPROTEIN-A1

Apo-A1 is the main component of High Density Lipoprotein (HDL), the "good" cholesterol. Apo-A1 constitutes about 70% of HDL content, defines its size and shape, and has a main role in lipid solubilization in HDL, cholesterol homeostasis and reverse cholesterol transportation (27). Its role in this transportation is due to Apo-A1 being a cofactor of Lecithin Cholesterol Acyl Transferase, which promotes the transport of cholesterol from tissues to the liver for excretion (28). This excretion is a contributing factor for atherosclerosis prevention, as it inhibits fat accumulation in white blood cells. This has been shown in a recent work (29) where Apo-A1 and HDL found in human atheroma (degenerative material found on artery walls) were oxidized and found to lose their ability

to excrete cholesterol, initiating the atherogenesis process, and increasing cardiovascular disease risk (30).

Apo-A1 was also shown to have an important role in the inhibition of cognitive loss caused by Alzheimer's disease. Apo-A1 can bind to Amyloid-β, a protein that is toxic to nerve cells causing cognitive deficit, attenuating its effects, and showing an anti-inflammatory effect in the brain (31). Apo-A1 is mainly produced in the liver and intestine. However, it is still able to cross the blood-brain barrier and is present in cerebrospinal fluid and brain. Because of this, breaks in cholesterol homeostasis can be associated with Alzheimer's disease (32).

Anti-bacterial effects were also shown to be expressed by Apo-A1. Apo-A1 and antibacterial activity levels in serum highly increased when bacterial preparations were injected in mice, as well as showing toxin-neutralizing activity. Anti-viral activity is also expressed, although not totally understood, possibly by Apo-A1 being involved in viral inactivation, disrupting viral entry into the cell or inhibiting virus cell fusion (33).

More recently, Apo-A1 was shown to have anti-tumour activity. Rather than directly inhibiting tumour cell growth, Apo-A1 affects the innate immune system by decreasing a tumour-permissive environment, reducing the expression of survivin, a protein that contributes to tumour proliferation by promoting cell-cycle activity. Apo-A1 also affects the adaptive immune system by inducing the expression of macrophages with anti-tumorigenic phenotypes (34). In addition, Lysophosphatidic Acid, which presents tumour proliferation activity, is cleared from serum by binding to Apo-A1, and this clearing activity is downregulated in ovarian, gastric and pancreatic cancer patients, indicating that Apo-A1 has an important role in clearing pro-inflammatory phospholipids like Lysophosphatidic Acid (35).

These are just a few of the vastly reported immunomodulatory effects of Apo-A1 and HDL activity in biochemical processes of immunity, inflammation, viral and bacterial infection and tumour proliferation. However, there are not many reports of the use of the affibody ZZapo for Apo-A1 recognition. Further understanding the mechanisms Apo-A1 is involved in, as well as studying the advantages of using the ZZapo affibody for its capture could provide promising advances in Apo-A1 targeted therapeutics and diagnostics.

3 POINT-OF-CARE TESTING

Molecular diagnostics focuses on the diagnosis of pathologies through biomarker detection or quantification. These biomarkers can be products of microbial or bacterial activity, viral RNA or enzymes and antibodies, but the most used biomarkers are proteins (36). Immunoassays, which use antibodies to capture a specific target, are the most popular choice for protein detection and quantification, they are well studied, can be used for a large number of antigens and are highly sensitive (1). However, these methods can result in slower diagnostics, may require experienced personnel and be costly due to the molecular components of these immunoassays. These are big disadvantages of this method, especially in resource limited settings (37).

The World Health Organization suggests diagnostics in resource-limited settings should be ASSURED: Affordable, Sensitive, Specific, User-friendly, Rapid and robust, Equipment-free and Deliverable. This is where Point-of-Care (POC) testing becomes most relevant (38). POC testing has been defined as *patient specimens assayed at or near the patient with the assumption that test results will be available instantly or in a very short timeframe to assist caregivers with immediate diagnosis and/or clinical intervention* (39). POC testing has emerged as a solution to the problems associated with healthcare infrastructure in developing countries, such as lack of resources and qualified personnel. It has the potential of delivering diagnostic results rapidly, while also being simple, inexpensive, disposable and portable, which is very attractive in resource limited settings (40,41). According to the Food and Drug Administration (FDA), a simple test has to be user-friendly in a way that it should be easy to use and doesn't require additional equipment or calculations/interpretation of the results to be read (detailed characteristics in Table 1). Some examples of currently available POC tests are blood glucose monitoring, pregnancy tests, arterial blood gas and HIV tests, which are all simple to conduct and for result interpretation (37).

Microfluidic technologies are a rapidly advancing field with great relevance in POC testing, as they allow the development of solutions for sample processing, assay performance and analyte detection at small scales. They exploit the small size of channels to promote the movement of micro quantities of fluids (39,42). There are plenty of microfluidic devices available already today, which can be classified depending on their mode of operation. Dipstick, cartridge and lateral flow are the types that stand out. Dipstick tests consist of porous pads that contain reagents and use reflectance technology to give a semi-quantitative

estimate of the analyte, which can go up to ten tests at once. They can also be coupled with reading devices to reduce user error, or have several layers to separate the red cells of a blood sample (37). Cartridge tests consist of a cartridge and a signal reader. A sample of blood is placed in the cartridge which in turn is placed in a reader for measurement. This reader is different for each type of analyte to measure, for example a glucometer that measures glucose in blood. They utilize thin-film electrodes fabricated on silicon chips for the sample analysis. These chips have different electrodes for different analytes, for instance, urine tests measure the ammonium ions that are produced by the hydrolyzation of urea, whereas glucose tests measure hydrogen peroxide produced by the glucose oxidase reaction (43).

Table 1 - FDAs' definition of a simple diagnostic test. Adapted from Yager et.al. (44).

FDA's Definition of a Simple Test
Fully automated instrument or unitized, self-contained test
Uses direct unprocessed specimens/capillary blood (finger-stick), nasal swabs, or urine
Needs only basic, non-technique-dependent specimen manipulation, including any for decontamination
Needs only basic, non-technique-dependent reagent manipulation ("mix reagent A and reagent B")
Needs no operator intervention during the analysis steps, no technical or specialized training and no electronic or mechanical maintenance
Produces results that require no operator calibration, interpretation, or calculations
Produces results that are clear to read, such as positive or negative, a direct readout of numerical values, the clear presence or absence of a line, or obvious colour gradations
Has test performance comparable to a traceable reference method, as demonstrated by studies in which intended operators perform the test
Contains a quick reference instruction sheet written at the educational level of the user

Lastly, Lateral Flow Assays (LFA), which will be the focus of this work, consists of a strip of material with recognition biomolecules (e.g antibodies) anchored on precise locations along which the liquid sample along with the target analyte moves. This provides qualitative and semi-quantitative results (45). Although the most common LFA nowadays are being used for the measurement of glucose and pregnancy tests, which measure human chorionic gonadotropin (hCG) in urine (hormone produced by the placenta after implantation of the

egg), there are tests available for drugs and infectious diseases that are also highly accurate (37,45). Notable examples include the detection of *Citrus Tristeza* virus infection in leaves or fruits (46), influenza (47), cocaine, ketamine, methadone, amongst others (48). One lateral flow technology that has received great attention lately, due to its simplicity and low cost, are the paper-based microfluidic devices, which will be elaborated on in the next section. Most traditional LFA are made of materials like glass, silicone or polymers such as poly(dimethylsiloxane) (PDMS) and poly(methylmethacryalate) (PMMA), which require specific complex fabrication processes and also some extra devices such as pumping systems to move the sample through the test (49,50). On the other hand, LFA can be made of paper, a material that is cheap, highly available and easy to manipulate. Paper devices can be mass produced at a very low cost, making it an ideal platform for POC devices, as well as making it an attractive matrix for bioassays.

4 MICROFLUIDIC PAPER-BASED ANALYTICAL DEVICES

Microfluidic Paper-based Analytical Devices (µPADs) are LFA conducted on paper matrixes using micro volumes of samples and reagents. They have received great attention in recent years due to their advantages in POC testing due to the use of paper (51). When compared to traditional materials, paper matrixes can be read visually, do not require pumps for the sample flow and are cheap and widely available (Table 2).

Table 2 - Comparison of traditional and paper-based devices (52).

	Traditional	**Paper-Based**
Material Manufacture	Glass, Silicon, Polymers Channel Fabrication Surface Modification	Paper Hydrophilic Channels (paper) Hydrophobic Channel Barriers
Sample Driving Force	Pump	Capillary Force
Result Analysis	Reader	Reader or Visual

Paper fabrication is an important milestone in human history. However, and excluding the use of filter paper for pH determination, it wasn't until 1949 that the first reports of paper-based microfluidic devices appeared in the works of Muller and Clegg (53). These authors used a filter paper with a wax barrier and observed that the restriction of the sample sped up

its diffusion by capillarity on the paper. The first demonstration of paper-based microfluidics was made by Whitesides *et al.* in 2007 (54) for the fabrication of µPADs, and was highlighted as an emerging technology in 2009.

The two main types of materials utilized for the fabrication of Paper-Based Devices are cellulose fibres, such as filter and chromatography paper, and nitrocellulose membranes. The ones used for µPADs are cellulose fibres, whereas nitrocellulose, which is naturally hydrophobic and requires deposition of surfactants, is commonly used in dipsticks and other LFA, such as pregnancy tests (55,56). Paper has many advantages when compared to other materials, the most obvious ones being its wide availability, it's inexpensive, even for high-quality chromatography paper, easily disposable and biodegradable (57). It's also a great platform for diagnostics as cellulose is exceptionally biocompatible, it is a good filter, its porous structures facilitate lateral-flow assays without the need of pumps for sample flow and it can be covalently bound to proteins and other biomolecules. The fact that it is white is also a great advantage because it makes it a good medium for colorimetric tests (58), being the material of choice for this work.

The process of manufacturing µPADs consists of physical or chemical patterning of hydrophobic barriers onto sheets of hydrophilic paper, making hydrophilic channels that contain the sample which can be open or sealed (59). Table 3 contains a summary of the most common patterning techniques used in the fabrication of µPADs along with some advantages and disadvantages. These hydrophilic channels patterning techniques used in the fabrication of µPADs along with their advantages and disadvantages. Most techniques use physical methods for patterning the paper, except for plasma etching and Alkyl Ketene Dimer (AKD) printing. Most of the methods require some specific equipment for the patterning (usually specific printers), which can be a disadvantage. However, wax printing has further advantages of simple and fast fabrication while also being easily replicated for mass fabrication and having good resolution (57,59).

Table 3 - Main methods of µPAD barrier patterning and their advantages and disadvantages. Adapted from (57,59)

	Method	**Material**	**Advantages**	**Disadvantages**
Physical Deposition	Photolithography	Photoresist	Good Resolution	Expensive Equipment
	Plotting	PDMS	Cheap/Flexible	Needs Customized Plotter
	Ink Jet Etching	Polystyrene	Good Resolution	Needs Customized Printer
	Screen Printing	Wax	Simple	Low Resolution

	Wax Printing	Wax	Simple and Fast	Needs Wax Printer
	Laser Treatment	Silicone/Wax	High Resolution	Does not allow LFA
	Flexography	Polystyrene	No heat treatment	Needs several layers
Chemical Deposition	Plasma Etching	AKD	Cheap	Needs Custom Molds
	AKD Printing	AKD	Simple and Fast	Custom Printer

In recent years, there has been an increased interest in the development of different µPAD fabrication methods, which focus different strategies, such as using different barrier materials for increased solvent compatibility, various designs for flow control, and new porous materials for more resistance against aggressive reagents (60). A paper highlighted the use of pullulan as an alternative barrier material to the typically used ones (Table 3). This polysaccharide polymer was combined with wax to create omniphobic µPADs resistant to organic solvents (61). *Xu et al.*(62) shows that hydrophobic barriers can be patterned with materials as simple as *Sharpie* (permanent maker) ink, which was loaded into cartridges for ink jet printing. One of the components of theses inks, however, is ethanol, which evaporates and results in low shelf life. Hand drawn barriers were also demonstrated, due to their simplicity and portability. A group showed the possibility of combining biologically relevant reagents with graphite pressed into pellets to be used in mechanical pencils, which produced a longer lasting signal than the same signal in solution form (63). Another author highlighted the use of ink pens to create hand drawn hydrophobic barriers, by using a trichloro perfluoroalkyl silane in hexanes ink, since the trichloro silanes react with paper to create hydrophobic barriers. The latter µPADs showed great versatility and great performance in colorimetric and ELISA tests (64). However, since the objective of this work is to create a simple µPAD, the method of choice will simply be wax printing, since the necessary equipment is available and it's a simple and quick methodology for designing and producing the tests, it's easily adjusted and reproduced and has great potential for mass production.

4.1 WAX PRINTING

Wax printing can be used for most µPAD applications, and is best suited for production in large numbers. Its cost is estimated to be about 0.001$ per test, when using high quality chromatography paper (Whatman paper) (65). This paper is mostly used as it is hydrophilic, homogenous, pure, reproducible, biocompatible, available and inexpensive (57,65).

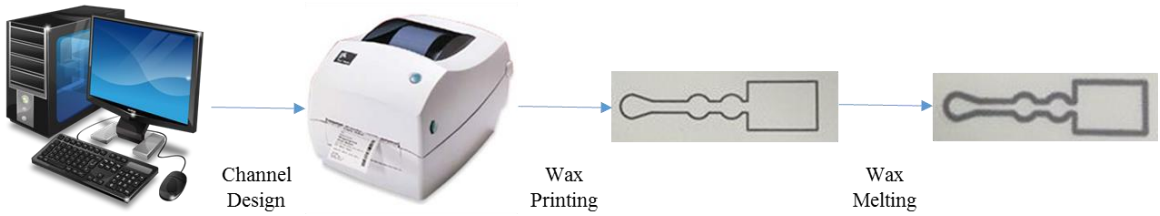

Figure 2 - Schematic representation of the three-step process of Wax Printed µPAD fabrication.

The process for µPAD fabrication consists of three steps: the channel design, wax printing of the channels, and melting the wax (Figure 2). First, the design of the channel is made using appropriate software, such as the AutoCad program. It is then replicated in a single sheet of paper and printed in a wax printer. If a wax printer is not available, wax dipping can also be used, which consists in using a plate or oven and molten beeswax to design the channels with an iron mold. However this technique presents the disadvantages of uneven penetration of the paper matrix and requires more control of wax melting temperature and time (66). Once printed, the paper is then heated on a plate or oven at 150ºC to melt the wax and allow it to diffuse through the thickness of the paper. As it is observable on Figure 2, the wax not only melts through the paper, but it also spreads laterally. This must be taken into account when designing the channels (65,67). Carrilho et. al (65) proposed an equation based on Washburn's equation to calculate this spreading:

$$L = \left(\frac{\gamma D t}{4\eta}\right)^{1/2}$$

In this equation, L is the distance where a liquid of viscosity η and surface tension γ penetrates a porous material with average pore diameter D in time t. From this, the width of the melted barrier is given by the equation:

$$W_B = W_P + 2L$$

Where W_B is the width of the barrier after melting and W_P is the width of the printed barrier (65). Even with its downsides, like low resolution of the devices, wax printing is still a fast, efficient and inexpensive method of fabrication that requires minimal knowledge to readily produce large amounts of µPADs with mostly elementary equipment (57,67).

4.2 SURFACE FUNCTIONALIZATION OF µPADS

Surface functionalization of µPADs is the process of coating the device with specific molecules selected to interact with specific targets. This is what makes biological assays in µPADs possible (55,68). The paper is said to be bioactive when those specific molecules are coating it. Bioactive paper has several applications, one of which is LFA assays, where a sample is introduced in one end of the paper and capillary forces move the sample through the test areas (56). Attachment of the molecules to the paper is not a strict requirement, as dry paper can sorb aqueous solutions and keep non-volatile components after drying. However, this opens the possibility of buffers or samples washing away the adsorbed molecules, and there is no control over the distribution of the molecules. This is problematic when working with expensive biosensors such as antibodies, enzymes, aptamers and nucleic acids (56,69). In addition, immobilization techniques can significantly influence shelf-life of µPADs, especially when they are exposed to changes in temperature during storage and transportation. *Nery et al.* (70) conducted experiments in enzyme-based µPADs to assess the influence of different immobilization methods in their stability and performance, noting that enzymes encased in polymers were found to be more stable when compared with direct adsorption. Additionally, an immobilization method using bilayer ionic polymer mixed with enzymes resulted in a higher enzymatic activity (70). As such, immobilization methods can be further adapted to improve shelf life.

Immobilization is indeed an important step in paper functionalization, and there are four main methods of doing it (Table 4), physical, using natural forces between the cellulose and biosensor, chemical, where reagents are manipulated to form covalent bonds with cellulose, biochemical coupling, in which molecules with affinity to cellulose are bound to biosensors, and finally bioactive pigments, that couple colloidal particles with biosensors that are applied onto the paper (56).

Table 4 - Main immobilization methods for paper functionalization and summary of their description (56)

Immobilization	**Description**
Physical	Biosensor adheres to the paper by van der Walls and electrostatic forces
Chemical	Covalent bonds fix the biosensor to the paper
Biochemical Coupling	Employs molecules that binds to paper and biorecognition molecules
Bioactive Pigments	Biosensors are coated on colloidal particles that are applied on the paper

Physical immobilization uses electrostatic and van der Walls forces to bind the biosensor molecules to the paper. However, since these forces are not very strong, the sensors are not strongly attached and can be washed away with washing buffers (56). For example, plasma proteins were shown to not strongly adsorb onto cellulose (71) and DNA with high molecular weight only adsorbs at pH 4 (72). Physical immobilization can be an easy method for some specific biosensor, however, it's not a great method, as they are not strongly anchored to the cellulose and there is no control over biosensor orientation (73,74).

Chemical immobilization uses covalent bonds to fix biosensors. Because pure cellulose doesn't have many functional groups, one must manipulate it to form these groups, usually with a polymer or a small molecule, in order to make bioconjugation possible (75). One work highlights the oxidation of regenerated cellulose to form aldehyde groups that react with amine groups on a DNA aptamer to form a Schiff base and reducing it, forming a covalent bond (76). Other works have shown other processes for different biosensors, like antibodies and enzymes. One of the main drawbacks of this process is the multiple chemical steps involved in the process, which makes it more complex time consuming and expensive (77,78).

Bioactive pigments consist in conjugating biosensors to colloidal particles, and then directly printing or spotting the whole structure onto the paper. It presents some advantages in comparison to other immobilization methods, such as the possibility of the complex coupling process being performed in specialized facilities and applied to the paper matrix later and to couple the colloidal particles with blocking and reporting functions (56,75). P(N-isopropylacrylamide) (PNIPAM) is commonly used in this method, because it has low non-specific protein binding (79). PNIPAM was also used in microgels coupled with DNA aptamers and antibodies, and stay immobilized on the paper matrix simply after spotting and letting it airdry (74). This method, however, does not allow correct orientation of the biosensors in the paper matrix, which could result in poor sensitivities and uneven visual signals (56).

4.2.1 Biochemical Coupling

The biochemical coupling method requires an intermediate molecule that binds the biorecognition molecule to the paper, which are applied directly to the test matrix by directly spotting the conjugate solution. The most commonly used ones in µPADs are the Carbohydrate Binding Molecules (CBMs), which have a high affinity to cellulose (75).

CBMs are defined as *contiguous amino acid sequence within a carbohydrate-active enzyme with a discrete fold having carbohydrate binding activity*. They are made up from 30 to 200 amino acids and can be a single, double or triple domain in one protein and can be found in either terminal of the polypeptide chain and sometimes in the centre. CBMs from different proteins have been found to have similar structures and they bind to cellulose because of their hydrophobic surface composed of several aromatic amino acids (80). Using this type of immobilization, it is possible to correctly position the biomolecule on the paper surface, allowing for a correct distribution of colorimetric signals (69). There are already several works that show the possibility of fusing of these CBMs with proteins, forming complexes that allow the specific immobilization of antibodies (81), proteins (82) and bacteriophages (83) onto a cellulose matrix. The fusion of CBMs with the Z-domain (previously mentioned in section 1) has already been shown as a good medium for immunoassays in µPADs with wax printed channels (69). Furthermore, this affibody-CBM conjugate can be produced from *E. coli*, reducing production costs by substituting an antibody with an affibody variant. For this reason, we will use this immobilization method in this work, using a fusion of a CBM with an Apo-A1 binding affibody as a capture conjugate for the capture immunoassay. Because immobilization methods alone do not provide quantitative or qualitative information, an appropriate detection system must be chosen to assess assay results.

4.3 DETECTION SYSTEMS

The detection or quantification of the analyte is a critical step for µPADs, as they are used for analytical purposes. Depending on what kind of molecule one is trying to detect, one must appropriately choose a detection system. There is a wide array of detection mechanisms that have been proposed for µPADs. The most well-established techniques are colorimetry, electrochemical detection and nanoparticle-based detection (52,84). Mass spectrometry, magneto-resistive sensors and nuclear magnetic resonance have also been applied in micro total analysis systems, however these are not as relevant for µPADs, as they employ expensive equipment (51).

Colorimetry is the most commonly used method for detection, as it is simple and cheap. This technique consists in using molecular or enzymatic dyes in the sample to react with previously immobilized reagents. These reagents can be enzymes, acid-base indicators or dyes (84). When a sample contacts a reaction zone, it results in a colour change that can

determine analyte levels using a calibration chart, which makes this method semi-quantitative. It also has the potential for multiplexing, which means, multiple reaction zones can be spotted in a single test (55). One paper highlights an excellent use of multiplexing for a titration of Ca^{2+} and Mg^{2+} in µPADs, as represented in Figure 3-A. It uses a single sample zone connected to ten reaction and detection zones with different concentrations of a chelating agent and a constant concentration of a metal indicator for colorimetric quantification (85). A distance-based multiplexed device was created to detect Ni, Fe and Cu in welding fumes. A ruler was printed onto the paper matrix to allow colour region length to be measured and quantified, allowing quick detection and quantification on site, which is represented in Figure 3-B (86). This methodology, however, presents a few disadvantages that are more evident when using micro volumes of reagents. Besides the small amount of sample used, buffers used in µPADs can wash away signalling components, which cause the signal colour to be spread unevenly and judgement of the colour can be challenging to the naked eye. This effect is not a problem for commercially available dipsticks, as there is a large amount of sample available (87). It can be time sensitive, since usually the colour of the dyes is only visible for a certain period of time before they become unreliable, and the results have to be read within that time window. Other dyes require some time to develop colour as well (37,55). Also, when a whole blood sample is used, red blood cells can make colorimetric reads difficult. However, spotting agglutination antibodies onto the µPAD before introducing the sample causes red blood cells to form aggregates too big to pass through the pores of the chromatography paper, while allowing blood plasma to sink into the paper (88). Furthermore, several layers of cellulose paper can act as a red blood cell filter (58).

Electrochemical detection uses electrochemical sensors printed onto the paper matrix in contact with the reaction zones, which, when a reaction occurs, send signals captured by electrodes that are converted in numerical values by a reader (52, 55,89). The sensors are made of three main electrodes, a counter electrode, a working electrode and one or more reference electrodes. These are printed on the paper matrix, typically with carbon inks for the counter and working electrodes, and with silver for the reference electrodes (55, 84,90). These devices have been shown to work for several analytes, such as lactate, uric acid (91), glucose (90), tumour markers (89), amongst others (58).

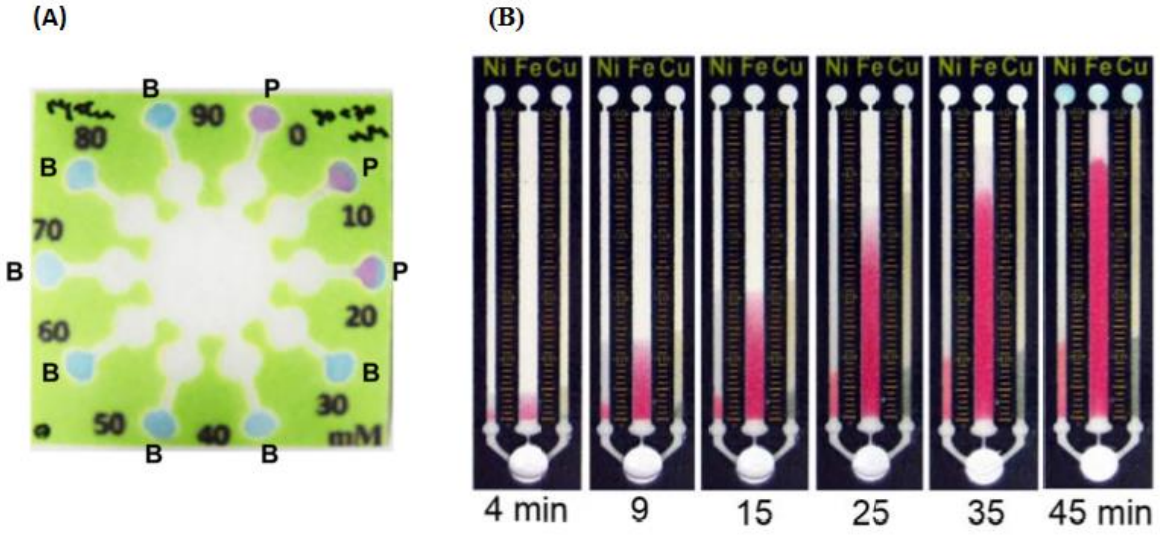

Figure 3 – Representation of two µPADs with colorimetric detection: (A) Titration of 30 mM of Ca^{2+} and 30mM of Mg^{2+} at pH 13, using solutions of Ethylenediaminetetraacetic acid from 0-90mM on the reaction zones, represented by the numbers next to the reaction zones. The colour of the zones is represented by the letters P (Purple) and B (Blue). The concentration of the analytes is determined in the zone where the is no colour change (30mM in this image) (85). (B) Distance-based measurement for Ni, Fe and Cu over a period of 45 minutes. Colorimetric reagents and buffers are printed onto the detection and pre-treatment zones, as well as a colorimetric indicator printed on the back of the device. The analytes were quantified when a metal-ligand complex precipitated on the substrate which generated a band of colour with length proportional to the amount of metal present. When the reaction ends, the coloured zones are measured with the printed rulers next to the detection zones for determination of concentration (86).

Since the concept of electrochemical detection is well known, it has become an attractive detection method for µPADs. It also has fast sensor responses and higher sensitivities. Furthermore, since they do not use colorimetric detection, they are not prone to incorrect visual reads and don't require removal of red blood cells. (55,91). More recently, there has been great interest in novel patterning and electrode materials, as well as modifying electrodes, for lower cost, greater sensitivities and better recognition (60). Metal nanoparticles have been shown to improve stability and conductivity and have already been incorporated in the fabrication of electrodes. This method, however can involve expensive fabrication equipment, which presents a disadvantage (92). Additionally, enzymes can also be used in electrochemical detection, but must be immobilized into cellulose adjacent to electrodes, as if they are on electrodes, they may impede electron transfer (93). While electrochemical detection is analytically superior to colorimetric detection, it is attributed to the use of signal detectors, which increase complexity and costs. Furthermore, the use of electrodes results in additional production steps and costs when compared to colorimetry (58). While hand-drawing electrodes is a possibility, they have limited reproducibility and are not suited for mass production. Nevertheless, they present a versatile tool for making well performing ePADs (94).

4.3.1 Nanoparticle-based Detection

Nanoparticles have already been shown to have great widespread use in cellulose and nitrocellulose-based paper platforms. While they can be used to improve electrochemical detection, they are generally used as a colorimetric method. They are attractive for detection purposes due to having higher stability and extinction coefficients than of common organic dyes, which means the colour is more intense and can be reliable for a longer period of time (55,84). They are also more sensitive, have lower detection limits and do not require a reader (95). AuNPs and monodisperse latex nanoparticles are commonly used in LFA, although AuNPs are preferred as they have more colour intensity and are smaller in size, and thus can easily adsorb into the paper in high densities, they are also easy to functionalize and are biocompatible (52,95,96). They possess a property that can be exploited for colorimetric detection, the Localized Surface Plasmon Resonance (LSPR). This property consists in the oscillation of the electrons in the gold atoms when they are exposed to light, polarizing the AuNPs and increasing their extinction coefficient, causing an intense colour (97). The size of the nanoparticles is an important factor when addressing colour intensity and particle stability, as bigger particles tend to have more sensitivity, however if they are bigger than 40 nm they are less stable. AuNPs smaller than 15 nm do not show an intense colour, and particles that are larger than 60-70 nm show self-aggregation if stored at 4ºC for several days (95). When the diameter increases, the LSPR shifts the colour to dark purple, this diameter increase can be caused by particle aggregation or by a controlled interaction, which can be exploited for colorimetric applications. This shift in colour has already been exploited to detect the bacteria *Mycoplasma pneumonia* (98) as well as prostate specific antigen and HIV-1 capsid antigen p24 (99) and other analytes, from nucleic acids to other small molecules at very low limits of detection, such as picomolar concentrations for proteins (97). Detection of *E. coli* was also shown on µPADs, AuNPs were coupled to lipopolysaccharide binding proteins, used to capture in a solution, and then transferred to paper. The presence of bacteria in the solution caused nanoparticles to aggregate, shifting colour from red to blue, with enough sensitivity to be applied to samples without amplification steps (116). Other works have shown the use of AuNPs as a detection tool for various clinically relevant biomolecules, environmental contaminants (100) and immunoassays (101,102). Furthermore, the use of hydrophobic barriers, such as wax barriers, on µPADs allows the fine-tuning of capillary flow and increasing the binding time between the analyte and the recognition molecule (97).

Since binding AuNPs to antibodies for immunoassays is a simple process (69), they have good reproducibility, can be finely tuned with different sizes for better signals and present fast results, they present an excellent tool for the optimization of POC devices, and will be the detection method used for this work.

5 CURRENT ADVANCES AND CHALLENGES

Throughout this introduction, several studies related to the development of µPAD technology were reported. Since these studies, several others have been conducted to further improve these devices. Because colorimetry is one of the most used detection systems in POC testing, it allows for the processing of data through smartphone technology. Using a smartphone camera, it is possible to measure colour intensity on a test and quickly analyse and display the signal (95,103). A few works already show the use of this methodology in LFA for the detection of drug abuse in saliva (48), quantification of vitamin D (104) and in µPADs (105). However, there are still problems related with ambient illumination that create fluctuations in the quality and reproducibility of smartphone captured images that need to be addressed.

Because these devices are made of paper, they can be easily manipulated and folded into three-dimensional (3D) devices, which is very advantageous for multiplexing and for more complex test matrixes, which gives them another focal point of interest (60). A 3D ePAD was created by *Wang et al.* which could be folded and unfolded to open or close the reaction zone for glucose electrochemical detection (106). The samples were introduced in the reaction zone when the device was open, let incubate for 2 minutes for enzymatic reaction to occur, and then it was closed to make contact with the detection zone and inserted into a glucometer, as represented in Figure 4. It was also shown to be useful in flow control as the sample only interacts with the detection when the user desires (106). Another much simpler 3D device was developed by *Camplisson et al.*, which consisted in a double ply channel made of wax. This channel was fabricated simply by stacking two single ply channels with a toner on the wax barriers, and then passed through a laminator. These channels showed a significant increase in flow speed at both 100% and 35% relative humidity in comparison to single ply channels (107).

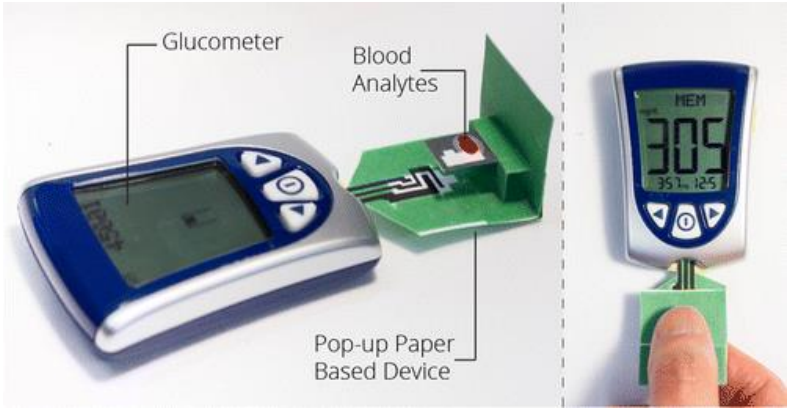

Figure 4 – Photograph of the 3D ePAD developed for glucose detection and quantification with the use of a glucometer. The blood sample is introduced in the reaction zone, where enzymes are stored, after 2 minutes of incubation, the device is closed, allowing the sample to make contact with the detection zone and producing a signal read by the glucometer (106).

Many authors aim to perform proof-of-concept experiments to show that certain analytes can be detected and quantified through µPAD technology. In recent years methodologies have been developed to extend µPAD use to several areas, like diagnostics, biochemical analysis, environmental monitoring, forensics and food quality control (108–111). A paper device was developed for simultaneous glucose and lactate testing in blood samples using enzyme-functionalized starch. These tests showed sensitivities in clinically relevant ranges, along with long shelf life at room temperature, proving that these assays do not require refrigeration (112). Another µPAD was developed to assess human male fertility using colorimetry. It exploits the use of diaphorase flavoprotein enzyme, present in healthy human sperm, to changing a reagent's colour from yellow to purple (113). Several tests relevant to environmental control have also been developed, such as an easy colorimetric test for on-site analysis, that consisted in chromatography paper patterned with wax to report the presence of Ni^{2+}, Cu^{2+} and Cr^{6+} in water samples, simply by dipping the device in the sample (114). 3D paper sensors for the detection of organophosphate and carbamate pesticides were also developed using acetylcholinesterase to convert indoxyl acetate into a blue-coloured product, which is inhibited in the presence of the pesticides (115).

Many experiments are also conducted to further show the versatility of µPADs, such as using them as a separation method. A report shows the capability of doing electrophoresis on µPADs for macromolecule separation, using a high electric field over a short distance (116). The devices were made of folded paper into thin layers, which allowed introduction and recovery of the sample by unfolding and cutting the layers of interest. It separated proteins from bovine serum rapidly and at low voltages (116).

Even though µPAD technologies are very promising for clinical applications due to their versatility and fine-tuneability, there are still many obstacles that need to be addressed, mainly related to their real world, out-of-lab applications. Most of their shortcomings are attributed to automation and standardization processes, especially when it comes to deposition of reactive components, as well as costs related to the molecular components of the assays, mainly of antibodies which represent most of the cost of lateral flow immunoassay devices (55, 95,103). Further exploring the use of alternative binding molecules, such as affibodies, could greatly reduce the costs of production of these devices and bring a greater interest for their further research and development.

6 OBJECTIVES

The main objective of this work is to study the possibility of developing a µPAD for detection of Apo-A1. For this purpose, a capture immunoassay was conceptually designed that combines a bi-functional protein fusion for antigen capture and a labelled antibody for detection. The protein fusion combines an affibody with affinity towards Apo-A1 (ZZapo) with the C-terminal of a family 64 Carbohydrate Binding Molecule (CBM) from *Spirochaeta Thermophile*. The CBM_{64} part recognizes the cellulose fibrils in paper (117), whereas the ZZapo module is able to recognize Apo-A1 (4). An Anti-Apo A1 antibody labelled with AuNPs is used for detection. A schematic representation of the Apo-A1 sandwich detection envisaged is shown in Figure 5-A. The µPAD is created on paper by using wax printing to define channels and reaction zones with a given geometry (Figure 5-B). To perform the Apo A1 detection, the ZZapo-CBM_{64} fusion is first anchored in the test zone. Then a certain volume of a test solution is dispensed on the sample zone of the device. These test solutions should include the Apo-A1 target coupled to the Anti-Apo-A1 antibody labelled with AuNPs. After migration of the test solution through the channel, the capture of the Apo-A1 antigen should be revealed by the accumulation of a red colour (from the AuNPs) over the test zone (Figure 5-B).

The first objective of this thesis was thus to produce and purify the fusion protein ZZapo-CBM_{64} in *E. coli*. Then, the cellulose and IgG binding properties of the ZZapo-CBM_{64} fusion will be tested and compared with the previously reported fusion ZZ-CBM_{64}, which uses the base affibody scaffold (ZZ), previously discussed in section 1, that binds to IgG via their Fc region (69). The next step is to design and produce a µPAD test with test

and control zones, for nanoparticle-based colorimetric detection, to optimize its design and study the interactions of ZZapo-CBM_{64}, with AuNPs conjugated with anti-Apo-A1 IgG and unconjugated AuNPs. The composition of the running buffer will also be optimized with the goal of minimizing non-specific interactions between the molecular components in the test. Then the capture assay will be conducted to test the capture and detection of Apo-A1, as illustrated in Figure 5. The test zone will contain the ZZapo-CBM_{64} fusion and the control zone a Goat Anti-Mouse IgG. The test should yield a qualitative result regarding the capture and detection of Apo-A1. On a positive test, the red colour in the test and control zones are a result of the accumulation of the conjugated AuNPs, which will be the result of a complexation of ZZapo-CBM_{64}, Apo-A1 and conjugated AuNPs in the test zone, and the capture of the conjugated AuNPs by the Goat Anti-Mouse antibody, for the validation of the test. If this capture and detection is successfully achieved, we will optimize the assay for a clinically relevant test, if not, we will try to ascertain the reason why the test is not working.

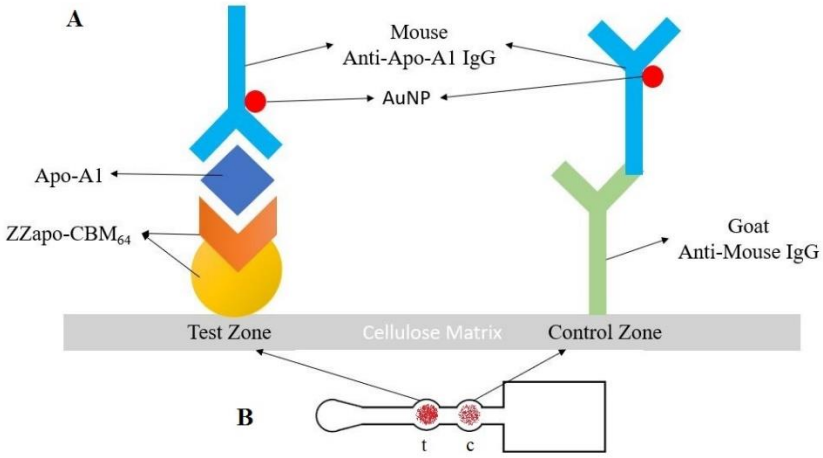

Figure 5 - Schematic representation of the envisioned sandwich assay of a positive capture µPAD test for the detection of Apolipoprotein-A1, using a channel with wax barriers, a ZZapo-CBM_{64} fusion in the test zone (t) and a Goat Anti-Mouse IgG in the control zone (c). A sample containing Apo-A1 and AuNP conjugated Anti-Apo-A1 antibodies is run through the channel of the µPAD test to form a ZZapo-CBM_{64}/Apo-A1/Anti-Apo-A1 complex in the test zone (t), and a Goat Anti-Mouse/Anti-Apo-A1 complex in the control zone (c).

7 MATERIALS AND METHODS

7.1 ZZAPO-CBM64 PRODUCTION

The recombinant protein ZZapo-CBM64, with specific binding capacity to Apolipoprotein-A1 (Apo-A1) which will be used as a model in this work, was cloned in a plasmid (pET21a; 5432 bp; Ampicillin resistance, Appendix A contains the final vector map) and produced in *Escherichia coli* by NZYTech. The protein fusion combines the N-terminus of a human Apo-A1 recognizing affibody (ZZapo) (4), a linker, the C-terminal of a family 64 Carbohydrate Binding Molecule (CBM) of *Spirochaeta thermophile* and a hexa-histidine tag. The corresponding 642 bp-long DNA sequence, which is represented in Figure 6, was cloned in the pET21a vector using the NdeI/XhoI enzymes, yielding a plasmid with 6074 bp. The sequence of the recombinant protein is represented on Figure 7.

```
CATATG
GATAACAAATTCAACAAAGACAAAAACAATGCAGCGGTGGAAATCATGCAACTGCCAAACCTTAATGCAGGCCAGATTT
TGGCCTTTATTATTTCCCTTCCGGATGATCCGAGCCAGAGCGCGAACCTGCTCGCGGAGGCGAAAAAACTCAACGATGC
GCAGGCACCGAAAGTTGATAATAAGTTCAATAAAGACAAAAATAATGCGGCGGTCGAAATTATGCAGCTTCCGAACCTC
AATGCGGGTCAGATCTTGGCCTTCATTATTTCGCTGCCGGATGACCCGAGCCAGTCGGCAAATCTGTTGGCGGAAGCGA
AAAAATTGAATGATGCACAGGCCCCGAAAGTCAGCTCTGGTCTGGTGCCGCGTGGCTCAACCGGCGAGTATACCGAAAT
TGCGTTGCCTTTTTCCTACGACGGGGCGGGTGAGTATTATTGGAAAACAGACGATTTCTCTACTACGACCAACTGGGGC
CGCTACGTCAATTCATGGAATTTGGATTTGCTCGAAATAAATGGCACTGATTATGCCAATACCTGGGTACCACAACATG
CCATCCCACCGGCCTCCGATGGCTACTGGTATATTCATTATAAAGGCTCATATCCGTGGTCGCATGTAGAGATGAAT
CTCGAG
```

NdeI
ZZapo
linker
cbm64
XhoI

Figure 6 - Gene sequence of ZZapo-CBM64 (*Spirochaeta thermophila*) (642 bp, GC%=48%)

```
MDNKFNKDKNNAAVEIMQLPNLNAGQILAFIISLPDDPSQSANLLAEAKKLNDAQAPKVDNKFNKDKNNAAVEIMQLPN
LNAGQILAFIISLPDDPSQSANLLAEAKKLNDAQAPKVSSGLVPRGSTGEYTEIALPFSYDGAGEYYWKTDDFSTTTNW
GRYVNSWNLDLLEINGTDYANTWVPQHAIPPASDGYWYIHYKGSYPWSHVEMNLEHHHHHH*
```

ZZapo
linker
cbm64
NdeI/XhoI
His-tag
Stop codon

Figure 7 - Recombinant protein sequence of the final ZZapo-CBM64 fusion (*Spirochaeta thermophila*). The molecular weight of the protein is of 24463.19 Da, as estimated by the Compute pI/Mw tool of the ExPASy Bioinformatics Resource Portal (https://www.expasy.org/).

For the protein production, competent *E. coli* DE3 strain BL21 cells (Novagen) were incubated with 1µL of the cloned vector and left on ice for 30 minutes, after which the cells were transformed by heat shock in a water bath (HAAKE DC10) at 42°C for 1 minute followed by 2 minutes in ice. The cells were then suspended in 1mL of pre-prepared Luria-Bertani (LB) broth from powder (Nzytech) for 1h at 37°C. Following this incubation, the cells were plated in a culture medium supplemented with ampicillin and left incubating overnight at 37°C. Liquid LB broth media was then prepared according to manufacturer's instructions and then autoclaved for 10min at 121ºC. The next day, a 30mL medium was supplemented with 100µg/mL of ampicillin and inoculated with a transformed white cell colony from the plated culture medium and cultured overnight at 37ºC at 260rpm. Its optical density (OD) was measured after the incubation at 600nm (OD_{600nm}) to determine the amount of culture needed to inoculate a 250mL medium and another 30mL medium, prepared in the same way, to an OD_{600nm} of 0.1. The calculated volumes were used to inoculate the 30mL and 250mL media, again supplemented with 100µg/mL of ampicillin, and incubated for about 1h, until an OD_{600nm} of 1 was achieved. Protein expression was then induced in the 250mL medium with 200µL of Isopropyl β-D-1-thiogalactopyranoside (IPTG) 1M (Fisher Scientific, BPΔ 755-10) and incubated for 6h at 37ºC, 260rpm. After the incubation, the culture was centrifuged at 4770rpm at 4ºC for 40min (Serial RCB, rotor SLC 3000). The supernatant was discarded and the pellet was resuspended in 1mL Tris-saline Tween 20 buffer (TST buffer: 50 mM Tris buffer, pH 7.6, 150 mM NaCl, 0.05% Tween 20). The cells were then sonicated on ice for mechanical cell disruption using Banollin-Sonoplus sonicator and a MS72 probe at 30W for 6min with 30s pulses and 30s intervals. The suspension was then centrifuged again at 8680rpm for 20min (Serial RCB, Sorval SS34), and the pellet was discarded.

The 30mL culture was used to create cell banks in vials of 200µL of glycerol 99% and 800µL of culture medium and stored at -80ºC, these were used at a later time to produce and sequence ZZapo-CBM_{64}. Using a 5mL LB broth medium, prepared in the same way as the previous ones supplemented with 100µg/mL of ampicillin, a cell bank was used to inoculate the medium and left at 37ºC, for about 2h, after which its OD_{600nm} was measured to calculate the volume needed to inoculate a pre-prepared medium of 250mL LB broth to an OD_{600nm} of 0.1. The rest of the protocol was the same as the previous one.

7.2 SEQUENCING OF ZZAPO-CBM$_{64}$

To evaluate if the produced vector had the expected sequence as presented in the report provided by NZYTech (Figure 6), vector sequencing was conducted. A cell bank of ZZapo-CBM$_{64}$ was cultured in a 5mL autoclaved LB broth medium supplemented with 100µg/mL of ampicillin overnight at 37ºC, 260rpm. The next day, plasmid DNA purification was achieved using a NZYMiniprep Kit (NZYTech MB01001) according to manufacturer's instructions. The resulting DNA pool was analysed in a NanoVue Plus spectrophotometer to ascertain its concentration and purity, which was 190ng/µL and Absorbance$_{260/280}$=1.939; Absorbance$_{260/230}$=2.065.

To confirm the presence of the ZZapo-CBM$_{64}$ sequence, two restriction enzymes that contained this sequence were selected for digestion of the plasmid, which were XhoI (Thermo Scientific) and XbaI (Promega). One sample of 500ng of the plasmid DNA was incubated with 2U XhoI, and another sample was incubated with both enzymes, at the same ratio, for 1h30 at 37ºC, with the "Buffer D" (Promega, pH7.9, 6mM TrisHCl, 6mM $MgCl_2$, 150mM NaCl, 1mM DTT) which was the common optimal buffer for both restriction enzymes. A 1% (w/v) agarose gel was then prepared in TAE buffer (40mM Tris, 20mM Acetic Acid, 1mM EDTA), the agarose (Fisher Scientific) was dissolved in the buffer, heated for 10 seconds at a time in a microwave and stirred until all the agarose was dissolved, poured into a mold and let cool until solid. Samples were mixed with a 6x loading buffer (40% sucrose (w/v), 0.25% Bromophenol Blue (w/v)) and loaded into the gel using a NZYDNA ladder III MW marker (NZYTech), which was run in TAE buffer at 100V for 1h. Gels were stained in an ethidium bromide solution (0.4µg/mL) and images were obtained with an Eagle Eye II gel documentation system (Stratagene) and processed in ImageLab.

The plasmid sequence was copied to the program SnapGene and 150 base pairs (bp) were selected before and after the ZZapo-CBM$_{64}$ sequence to look for primers, which were evaluated in the program Oligoanalyzer for quality and for likelihood of forming hairpins and dimers. Once the best primers were selected, the purified DNA was sent to Stabvida for sequencing. The provided sequence was then compared with the original ZZapo-CBM$_{64}$ sequence (Figure 6) for mismatches.

7.3 ZZapo-CBM$_{64}$ Purification and quantification

The fusion protein was purified by metal affinity chromatography with a Niquel Sepharose 6 Fast Flow column (HisTrap FF; GE Healthcare) in an ÄKTApurifier 10 system (GE Healthcare). The protocol used was according to manufacturer's instructions. Two buffers were used in the process, Buffer A (10mM Imidazole, 50mM NaHEPES pH 7.5; 1M NaCl, 5mM $CaCl_2$) and Buffer B (300mM Imidazole, 50mM NaHEPES pH 7.5; 1M NaCl, 5mM $CaCl_2$). The column was equilibrated with 5 column volumes of buffer A and the supernatant was loaded in the column. The unbound proteins were eluted with 20 volumes of buffer A and the ZZapo-CBM$_{64}$ protein was eluted with 10 volumes of buffer B.

To evaluate the purity of the purified protein, a Sodium Dodecyl Sulphate Polyacrylamide gel electrophoresis (SDS-PAGE) was performed. The polyacrylamide gels were synthesized with 12% acrylamide and bis-acrylamide total concentration and 3.3% of bis-acrylamide for the resolving gel, and 4% total concentration and 3.3% of bis-acrylamide for the stacking gel. The samples were prepared by adding 5µL of denaturing agent 1 M Dithiothreitol (DTT) (Sigma Aldrich), 25µL of 2x Laemmli Sample Buffer (Bio-Rad) prepared according to manufacturer's instructions and 20µL of purified sample. The samples were incubated for 10 minutes in a 100°C water bath and were then placed in gel. A 10-250kDa protein ladder (Bio-Rad, Precision Plus Protein Standards) was used as a molecular mass marker. The gel was run at 90V until the front of the gel reached the end of the gel plates. Coomassie Brilliant Blue was used to stain the gels and destaining was achieved with a 30% ethanol and 10% acetic acid solution. Images of SDS-PAGE gels were obtained with GS-800™ Calibrated Densitometer (Bio-Rad) and processed in ImageLab.

Quantification of the ZZapo-CBM$_{64}$ protein was achieved with the Bicinchoninic Acid (BCA) Protein Assay using the microplate procedure of Pierce® BCA Protein Assay kit (Thermo Scientific), prepared according to manufacturer's instructions.

7.4 Comparison of ZZapo-CBM$_{64}$ with ZZ-CBM$_{64}$

To evaluate efficiency and properties of the novel ZZapo-CBM$_{64}$, a few tests were conducted to compare it with a ZZ-CBM$_{64}$ protein (previously synthesized by a colleague using a method similar to the production and purification section described above). In this second fusion, the ZZ portion has a strong affinity to the Fc portion of antibodies.

To assess if the new construct has similar binding properties to cellulose 3 samples of 20pmol of both proteins were diluted to a final volume of 15µL using Phosphate Buffered Saline (PBS, 137mM NaCl, 10mM Phosphate, 2.7mM KCl, pH 7.4), and on the blank samples, 20µL of PBS was added. On the second set, 20µL of a 20µM micro-cellulose particles (Sigma-Aldrich Sigmacell Cellulose type 20 diluted in PBS) suspension was added and on the third set, a strip of Whatman no.1 chromatography paper was added (3mmx2mm) along with 20µL of PBS. These samples were incubated for 10min on a shaker (VWR Digital Vortex Mixer) at Room Temperature (RT) after which they were centrifuged at 2000g (VWR Ministar Silverline) for 5min and a 20µL sample of each test was submitted to SDS-PAGE (in the same conditions as described above). The gel was then stained with Silver Nitrate. First the gel was incubated on a shaker for 2h with a 30% ethanol and 10% acetic acid solution for fixation, followed by two washing steps, the first one with a 30% ethanol solution for 10min, and the second with MilliQ water twice for 10min. Then the gel was incubated for 1min with a 0.02% Sodium Thiosulfate solution, followed by 3 washing steps of the gel with MilliQ water for 30s. Staining was achieved by incubating the gel with a 0.15% Silver Nitrate Solution for 30min, followed by a washing step with MilliQ water for 1min. Colour development was achieved by using a 3% Sodium Carbonate and 0.05% Formaldehyde solution, the solution was poured onto the gel and shook until a brown precipitate formed, which was then discarded, and then fresh solution was poured onto the gel and shook until protein bands appeared. The colour development continues until a 5% Acetic Acid solution is added to stop the development. The gel was then washed with MilliQ water, scanned with GS-800™ Calibrated Densitometer and processed in ImageLab.

The ZZ module in the ZZ-CBM_{64} fusion is able to bind to IgG antibodies (69). To check if ZZapo module, which is derived from a ZZ module, in the ZZapo-CBM_{64} fusion lost the IgG binding capacity, as required, another experiment was conducted. Both fusions were diluted to 10µM and spotted onto the control and test zones (ZZ-CBM_{64} and ZZapo-CBM_{64} respectively) of the final µPAD design (Figure 8) using a 40nL needle (Schleicher & Schuell MicroCASTer 8-Pin System), the needle was washed in 5% Bleach, MilliQ water, 70% Ethanol and MilliQ water again. 10µL of PBS buffer was then used to wash the channel, followed by 15µL of IgG marked with Fluorescein Isothiocyanate (FITC 0.01µM) and incubated in the dark for 20min, washed again with 10 µL of PBS, and incubated in the dark again for 20min. The paper strips were then analysed in a microscope (Leica I3 Filter Cube,

LEJ EBQ 100 isolated power supply) and pictures were snapped using the software cellSens with an Olympus XC30 microscope camera.

7.5 PREPARATION OF µPADS AND AUNPS

The paper utilized in all the tests was Whatman no.1 chromatography paper (Product number: 3001-878; Whatman™, GE Healthcare©), in 250x250mm sheets with a thickness of 0.18mm, cut into A5 sheet size to fit the wax printer. The channels were designed using the software AutoCAD, which allows the design of precise 2D and 3D models. The patterns were designed black against a white background. The dimensions of the final channel design are represented on Figure 8. This channel allowed enough space for 0.5µL of sample in the test spots at once and showed an efficient flow of liquid, the thickness of the wax line is 0.4mm. For spot assays, the channels had 8mm in diameter. For test velocity assays, the channels were 4.5cm long, 0.3cm wide and the spots had 0.6cm in diameter.

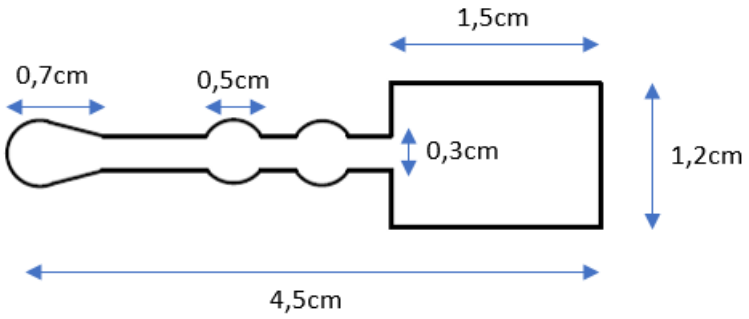

Figure 8 - Final design and dimensions of the µPAD channels used in tests.

The channels were printed using a Xerox ColorQube 8570 colour printer that prints wax. The print head dispenses ink (melted wax) on the surface of the paper, where it cools and solidifies instantaneously without further spreading. The components of the ink which are mainly hydrophobic carbamates, hydrocarbons and dyes, have a melting point around 120°C. To melt these channels, two methods were used. The first one consisted in applying the paper directly onto a magnetic/heating plate (IKA RCT Classic) at 150ºC for about 2min, or until the wax was visibly melted through the paper uniformly. The second method was performed using an oven (BINDER FDL 115) at 150ºC and placing the sheets of paper on the racks for about 3-5min, which was a more convenient method as considerably more tests could be done at once, and the heat was evenly applied, allowing for a more even melting and spreading of the wax. Some tests use an adhesive membrane (Adhesives Research

Ireland Ltd; MH-93241-2) to cover the bottom of the paper strips, which allows for tests to be done on top of surfaces, as opposed to suspended.

Gold nanoparticles (AuNPs) were prepared using the Naked Gold Conjugation Kit 20nm and 40nm (BioPorto Diagnostics) according to manufacturer's instructions for a pH of 7.8 using 4nm particles, which were conjugated with a mouse Anti-Apolipoprotein-A1 IgG (Anti-Apo-A1, AntibodyShop). Unconjugated AuNPs were prepared the same way, using a volume of MilliQ water equal to the one used for antibodies in conjugated AuNPs, as well as stabilizing buffer to avoid aggregation of the nanoparticles. The process was done successfully if the solution remains red (Figure 9-A), or unsuccessfully if the solution turns grey, which indicates particle aggregation (Figure 9-B).

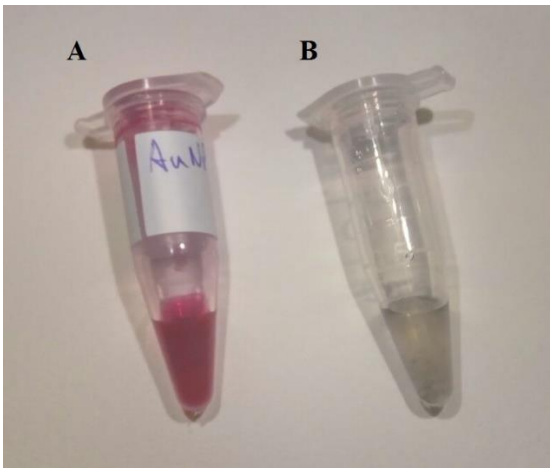

Figure 9 – (A) Successfully antibody-conjugated AuNPs; (B) Unsuccessfully conjugated agregated AuNPs.

All µPAD tests were done using 5pmol of ZZapo-CBM_{64} and Goat Anti-Mouse IgG pre-deposited in the test and control zones, respectively. The sample for Apo-A1 tests contained 10pmol of Apo-A1, along with 3µL of Anti-Apo-A1 antibody conjugated AuNPs, then running buffer is added to a total volume of 12 µL, incubated for 5min and added to the sample zone of the channel. When the tests do not contain Apo-A1, the same volume of AuNPs is used and 9µL of running buffer is added to a total volume of 12µL. A test where both the control and test zones of the µPAD show a signal is considered a positive test. If only the control zone has a signal, the test is considered negative. If the test zone presents a signal, but the control zone does not, the test is considered invalid. The control zone contains a Goat Anti-Mouse IgG (Ab-Goat, Nal Von Minden). The antigen detection was done using Human Apo-A1 (Sigma-Aldrich) as a model. All tests were ran in triplicates for more reliable results.

7.6 EVALUATION OF ZZAPO-CBM$_{64}$ CAPTURE OF APOLIPOPROTEIN-A1

The ability of the ZZapo-CBM$_{64}$ fusion to capture Apo-A1 by was evaluated with two methodologies. First, a Basic Native Gel was done. The gel was prepared with a 10% acrylamide and bis-acrylamide total concentration. Samples of 15pmol of ZZapo-CBM$_{64}$, Apo-A1 and Anti-Apo-A1 monoclonal antibody were diluted to a final volume of 15µL, let incubate for 10min and then 10µL of loading buffer (40% Glycerol, 12.5% 0.5M Tris-HCl pH 6.8, bromophenol blue traces) was added to the samples, which were then loaded onto the gel. It was run at 80V for 3h30 in running buffer (0.6% Trizna, 2.6% Glycine, pH 8.9) and then stained with Silver Nitrate, as described in the previous section. The gel was then washed with MilliQ water, scanned with GS-800™ Calibrated Densitometer and processed in ImageLab.

To further confirm the results from the Native Gel, another experiment was conducted using cellulose microparticles like the one described in the previous section. Samples of 20pmol of ZZapo-CBM$_{64}$, Apo-A1 and Anti-ApoA1 monoclonal antibody were diluted to a final volume of 15µL using PBS and let incubate for 10min at RT on a shaker (VWR Digital Vortex Mixer), after which 20µL of a 20µM micro-cellulose particles (type 20 diluted in PBS) suspension was added and incubated again for 10min on a shaker at RT. The mixture was then centrifuged at 2000g for 5min and a 20µL sample of each was submitted to SDS-PAGE, as described in section 7. The resulting gel was stained with Silver Nitrate washed with MilliQ water, scanned with GS-800™ Calibrated Densitometer and processed in ImageLab.

8 RESULTS AND DISCUSSION

8.1 DESIGN, CONSTRUCTION AND SEQUENCING OF ZZAPO-CBM_{64}

The first goal of this thesis was to design and construct a bi-functional protein fusion that combines a ZZapo affibody with affinity towards Apo-A1 with a CBM_{64} from *S. thermophile* with affinity towards cellulose. The sequence of the corresponding gene was designed on the basis of the sequences found in the literature (4,117). A hexa-histidine tag was included in the fusion to facilitate purification (Figure 6 and 7). The cloning of the desired sequence in a pET21a plasmid was outsourced to NZYTech. *E.coli* cells were then transformed with the resulting construct. The plasmid was then amplified by growing cells, purified using a NZYMiniprep Kit and sent to sequencing to confirm cloning. A plasmid solution with a concentration of 190ng/µL and ratios of absorbance of 1.939 for Abs_{260}/Abs_{280} and of 2.065 for Abs_{260}/Abs_{230} was obtained from the NZYMiniprep Kit. The Abs_{260}/Abs_{280} ratio indicates protein contamination in nucleic acids, and in pure DNA should be around 1.8; thus, the obtained purified DNA, which showed a Abs_{260}/Abs_{280} ratio of 1.939, does not have significant protein contaminations. The Abs_{260}/Abs_{230} ratio indicates contamination of organic compounds, and should be around 2.0 for pure DNA; thus, the obtained purified DNA, which showed a Abs_{260}/Abs_{230} ratio of 2.065, is not contaminated by organic compounds.

In order to confirm if the plasmid construct contained the ZZapo-CBM_{64} module (Figure 6), one sample of purified DNA was incubated with the restriction enzymes XhoI and XbaI, and another sample was incubated with just XbaI. These enzymes should cut the plasmid in an unique site, and when acting together should isolate the ZZapo-CBM_{64} module (800 bp) from the vector backbone. Digested samples, along with a MW marker and an undigested plasmid were analysed by electrophoresis in a 1% agarose gel, which was stained with ethidium bromide (Figure 10). The undigested plasmid in lane 2 is characterized by two bands, which correspond to the relaxed (>10000 bp) and supercoiled (~5000 bp) isoforms of the plasmid. As expected, the DNA sample digested with XbaI in lane 3 contains a single band (~6100 bp), which corresponds to the linearized form of the plasmid. Lane 4 contains the DNA sample digested with both XhoI and XbaI. A first band with <6000 bp is seen that corresponds to the vector backbone. This band migrates slightly faster than the one observed in Lane 3. A second band is barely visible at 800bp that corresponds to the excision of a

fragment containing the ZZapo-CBM_{64} module by both restriction enzymes. These results confirm that a fragment in the plasmid with a size and location compatible with the ZZapo-CBM_{64} is present. Furthermore, the linearized form (lane 3) migrates slower than the major band observed in lane 4, since the latter has an excised fragment, which was expected. Even though the isoforms present in lane 2 have the same weight, their conformations are different. The supercoiled form migrates faster than the relaxed since it more easily moves through the gel.

Having confirmed that a fragment is present in the plasmid with a size and location compatible with the ZZapo-CBM_{64} module, the purified plasmid DNA was sent for sequencing to Stabvida with two primers that were selected about 150bp before and after the sequence. The sequence was obtained in both forward and reverse sequencing to confirm possible mismatches. If errors emerge that are present in both sequences, then the mismatch must be real. The quality of the sequencing data is represented in Figure 11, where the first graph is the Forward sequence, and the second is the Reverse sequence.

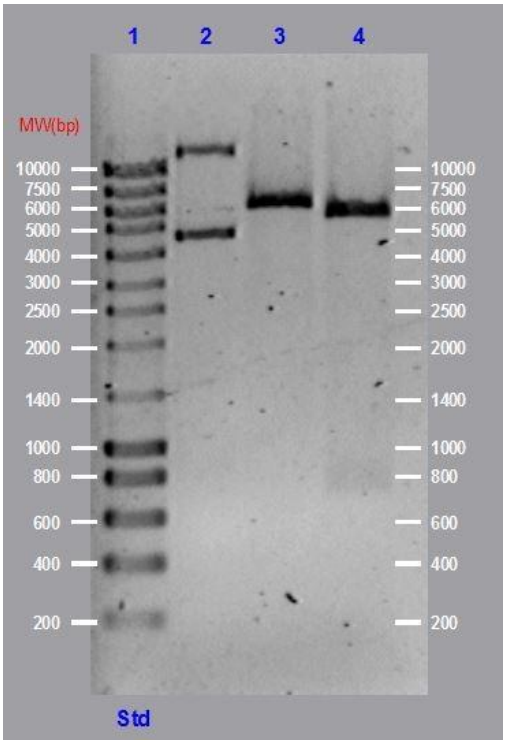

Figure 10 – Agarose gel stained with ethidium bromide of: 1) Molecular weight marker; 2) Undigested purified plasmid; 3) Purified plasmid digested with XbaI; 4) Purified plasmid digested with XhoI and XbaI.

Figure 11 – Quality of sequencing data provided by Stabvida of the forward sequencing (first graph) and reverse sequencing (second graph).

As previously mentioned, the sequence of interest starts at about 150bp in both the forward and reverse sequences, where the primers were selected. In both graphs of Figure 11 we can observe that the first 100bp of each sequence have considerably lower quality than the following bps, and the reverse sequence (second graph) has a better overall quality than the forward sequence (first graph). Both sequences were analysed in Olygoanalyser for mismatches with the original ZZapo-CBM$_{64}$ module sequence, which did not show any mismatches in this area (Figure 12).

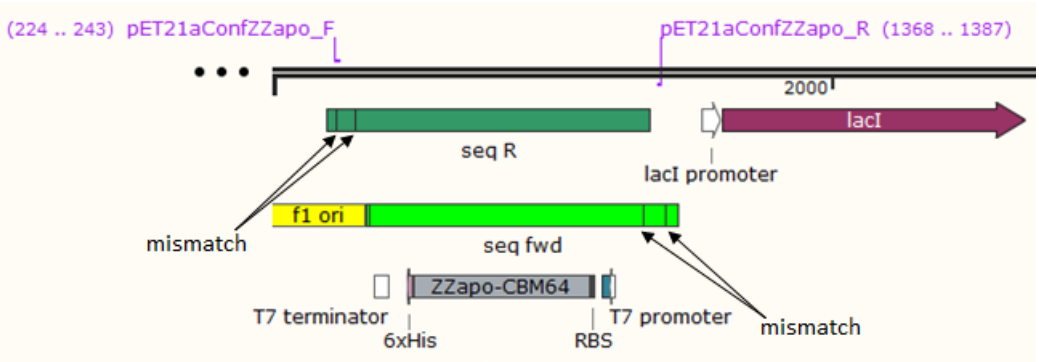

Figure 12 – Representation of the sequences obtained by Stabvida, seq R is the reverse sequence, seq fwd is the forward sequence, ZZapo-CBM64 is the sequence of the original ZZapo-CBM$_{64}$ module in the plasmid. Mismatches of the seq R and seq fwd sequences are marked with black lines in these sequences.

The data from all the sequences is shown in Figure 12 where seq R is the reverse sequence, seq fwd is the forward sequence and ZZapo-CBM$_{64}$ is the original ZZapo-CBM$_{64}$ module sequence (Figure 6). The bars representing each sequence are aligned, meaning that

the location of the bars represent the location of the actual sequence. The black lines in the forward and reverse sequences correspond to mismatches. Since these mismatches were not found simultaneously in the forward and reverse sequences, the mismatches are not real. Furthermore, the part containing the ZZapo-CBM_{64} sequence did not show any mismatches, confirming that the produced ZZapo-CBM_{64} had the expected sequence. Thus, any eventual inability of ZZapo-CBM_{64} to capture Apo-A1 will not be attributable to an incorrect synthesis of the ZZapo-CBM_{64} construct.

8.2 PURIFICATION AND QUANTIFICATION OF ZZAPO-CBM_{64}

Protein purification was achieved by using metal affinity chromatography with a Niquel Sepharose 6 Fast Flow column in an ÄKTApurifier 10 system. This column was used because the fusion protein contains an exposed Histidine tag in its C-Terminus, which forms complexes with Ni^{2+} ions immobilized in the resin, allowing the selective binding of these proteins. Imidazole is a competitive binder to the ions, and is used in all the elution buffers, although in low concentrations, to avoid or wash away non-specific binding. The elution buffer has a higher concentration of imidazole to elute away the purified protein, as it competitively binds to the ions in the resin. Figure 13 shows a chromatogram of a representative run of ZZapo-CBM_{64} purification. Two major peaks of absorbance at 280nm are noted. The first corresponds to the flow of unbound proteins that didn't bind specifically to the Ni^{2+} ions, whereas the second peak corresponds to the elution of ZZapo-CBM_{64}, which was separated in two pools. The pool with higher concentration (Fraction A) was recovered from the fractions 23mL to 26mL, and the second pool (Fraction B) was recovered from the fractions 26mL to 34mL. Fractions A and B are highlighted in Figure 13 in red and green respectively. The first fractions of purified ZZapo-CBM_{64} recovered after the chromatography had a higher concentration, as confirmed by the peak in Abs_{280nm} highlighted in a red rectangle in Figure 13. However, the protein was continually eluted at lower concentrations until the end of the run (highlighted in a green rectangle in Figure 13). Since we wanted a concentrated ZZapo-CBM_{64} solution, we separated the eluted protein fractions in two pools, A and B, so as not to dilute the highly concentrated fractions. Other purification runs were done when the pools of ZZapo-CBM_{64} ran out. These runs had a similar chromatogram (results not shown).

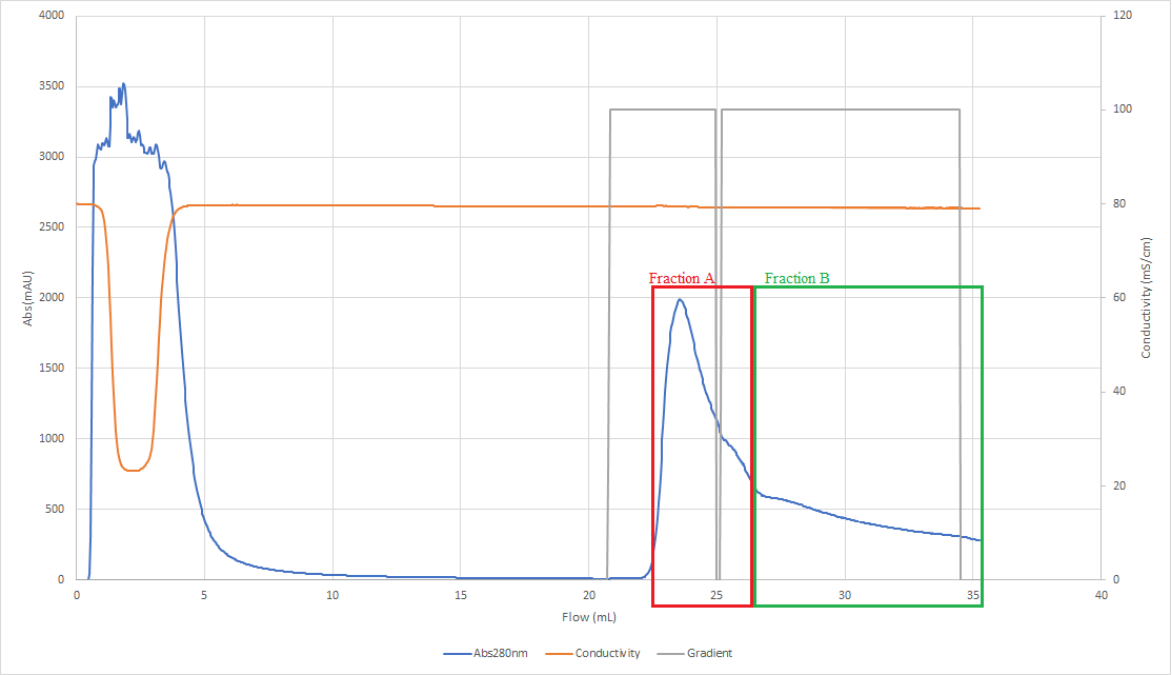

Figure 13 - Purification of ZZapo-CBM$_{64}$ fusion was achieved by metal affinity chromatography with a Niquel Sepharose 6 Fast Flow column. The column was equilibrated with 5 column volumes of buffer A (10 mM Imidazole, 50 mM NaHEPES pH 7.5; 1 M NaCl, 5 mM CaCl2) and the clarified E.Coli lysate was loaded in the column. The unbound proteins were eluted with 20 volumes of buffer A and the ZZapo-CBM64 protein was eluted with 10 volumes of buffer B (300 mM Imidazole, 50 mM NaHEPES pH 7.5; 1 M NaCl, 5 mM $CaCl_2$). The chromatogram was obtained by reading the absorbance at 280 nm. The second peak in the Abs280 line corresponds to the eluted fusion protein. The recovered Fractions A and B are highlighted in red and green respectively.

To evaluate the purity of the extracted fractions, an SDS-PAGE was performed. The resulting gel is shown in Figure 14. The first lane in the gel of Figure 14 corresponds to a 250kDa molecular weight standard (Bio-Rad). Lane 2 is a sample of the cell lysate containing the fusion protein loaded into the Niquel Column. Lane 3 represents a sample of the first fractions collected in the elution (first 5mL from elution). Lanes 5 and 7 are a sample of the purified ZZapo-CBM$_{64}$ fractions A and B respectively (24.47kDa), which show no other impurities in the gel. The band represented in lane 7 is smaller due to its lower concentration. For comparison purposes, lane 9 was run with a purified ZZ-CBM$_{64}$ sample, which is slightly lighter than the other construct (24.16kDa). The remaining lanes were filled with loading buffer diluted in the same volume as the samples, to avoid stretching of bands due to density differences.

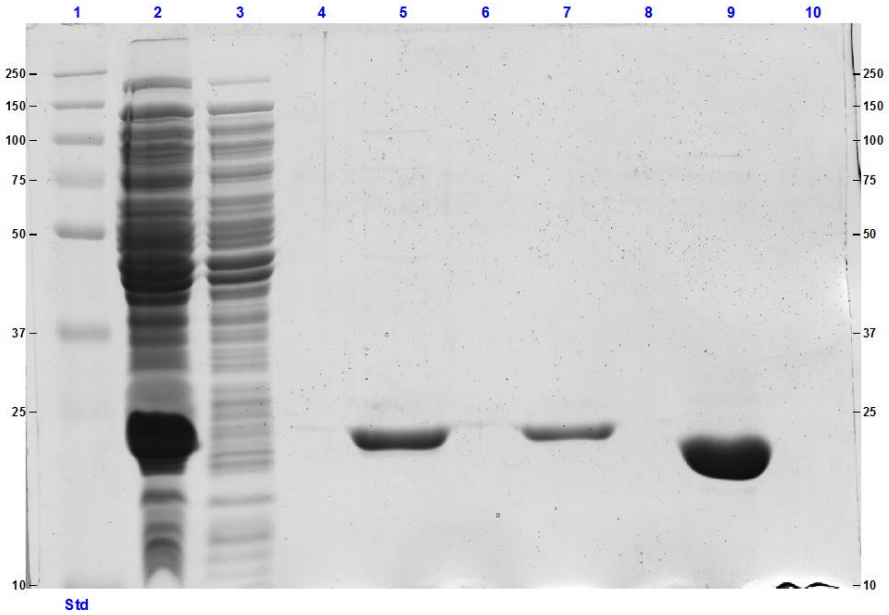

Figure 14 - Coomassie Blue Stained SDS-PAGE analysis of the purification of ZZapo-CBM$_{64}$ Lanes: 1) 250kDa molecular weight standard; 2) E.Coli lysate sample loaded onto the Niquel Sepharose 6 Fast Flow column; 3) Flow-through sample; 5) Purified ZZapo-CBM$_{64}$ faction A; 7) Purified ZZapo-CBM$_{64}$ faction B; 9) Purified ZZ-CBM$_{64}$.

To quantify the protein in fractions A and B, the BCA Assay was used. Bovine Serum Albumin Standards of known concentration were prepared in the Buffer B used in the purification of the construct to avoid any differences in absorbance caused by the difference of buffers, read at 562nm along with purified fractions A and B and plotted and linearized (Figure 15).

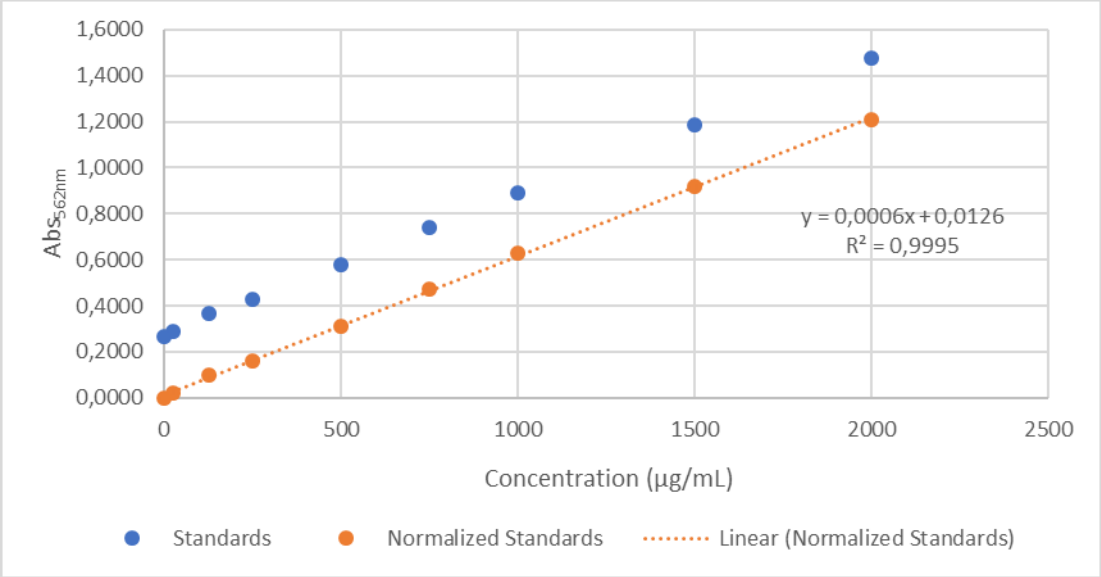

Figure 15 - Graphic representation of the prepared BSA standards concentrations versus their Absorbance at 562nm, along with the normalization of those values and its linearization, equation of the linearization and Coefficient of Determination (R^2).

Using the equation provided by the linearization, the concentration of fractions A and B were calculated using their Abs_{562nm}. The calculated concentrations were 320.7µg/mL and 80.3µg/mL respectively, which correspond to a molarity of 13.1µM and 3.28µM respectively. The Coefficient of Determination (R^2) value is also a good indicator that the determined linearization was accurate.

8.3 COMPARISON OF ZZAPO-CBM64 WITH ZZ-CBM64

The ZZapo affibody was derived from the ZZ module by changing a number of amino acids in such a way that the affinity of ZZ towards the Fc portion of IgG antibodies is lost and the affinity towards Apo A1 is obtained (4). A few tests were thus conducted to check if the new ZZapo affibody retained some of the ability of the ZZ module to recognize IgG antibodies. These tests were performed using the ZZapo-CBM_{64}, and ZZ-CBM_{64} constructs. The ability of the CBM_{64} modules in the fusions to bind to cellulose was also assessed.

First, the cellulose binding capacity of the CBM_{64} portion was assessed by incubating the fusions with cellulose microparticles or a piece of cellulose paper separately, centrifuging the mixtures and analyzing the supernatant by SDS-PAGE. The binding of the fusions to cellulose during the incubation should produce a supernatant free of protein upon centrifugation. The SDS-PAGE analysis of then resulting centrifuged supernatants is shown on Figure 16. Lanes 1 and 2 of the gel correspond to ZZ-CBM_{64} and ZZapo-CBM_{64} respectively, before adding cellulose, for control. Lanes 4 and 5 represent the centrifuged supernatant obtained after incubation of ZZ-CBM_{64} and ZZapo-CBM_{64} respectively with cellulose particles, and lanes 7 and 8 represent the centrifuged supernatant obtained after incubation of ZZ-CBM_{64} and ZZapo-CBM_{64} respectively with cellulose paper. Because no protein was detected on lanes 4, 5, 7 and 8, we can assume that the molecules were captured by the cellulose in both cases. This is in accordance with the expected results, proving the high affinity of the ZZapo-CBM_{64} and ZZ-CBM_{64} constructs to cellulose. The remaining lanes were filled with loading buffer to avoid stretching of bands due to differences in density. All lanes show 2 bands on the initial part of the gel, which could be caused by some impurity present in the loading buffer, due to improperly washed material or some contamination during the preparation of the loading buffer.

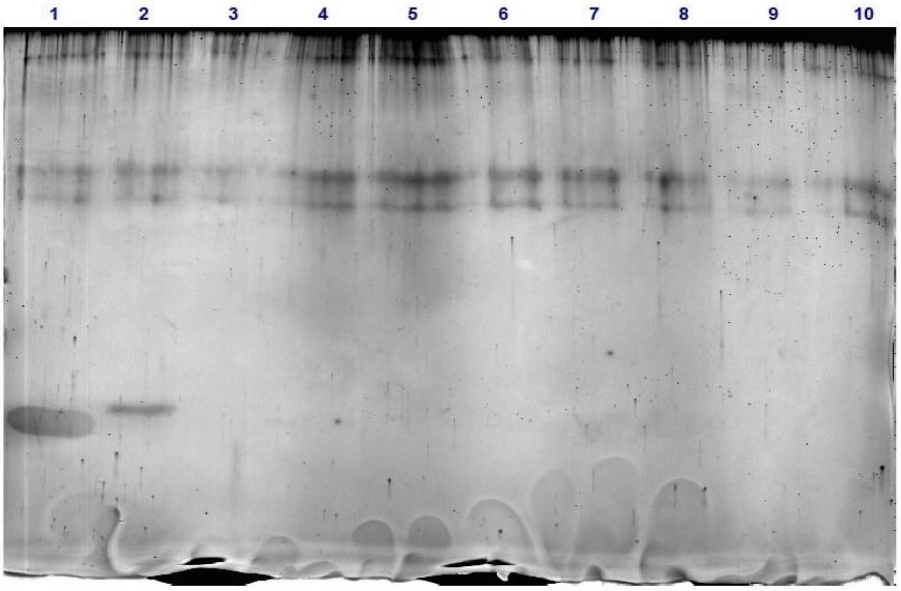

Figure 16 - Testing of the affinity of ZZ-CBM$_{64}$ and ZZapo-CBM$_{64}$ fusions towards cellulose. Cellulose microparticles and cellulose paper were incubated with the fusions and removed by centrifugation. The supernatants were then analysed by SDS-PAGE. Lanes: 1) ZZ-CBM$_{64}$; 2) ZZapo-CBM$_{64}$; 4) Supernantant of ZZ-CBM$_{64}$ incubation and centrifugation with cellulose particles; 5) Supernantant of ZZapo-CBM$_{64}$ incubation and centrifugation with cellulose particles; 7) Supernantant of ZZ-CBM$_{64}$ incubation and centrifugation with cellulose paper; 8) Supernantant of ZZapo-CBM$_{64}$ incubation and centrifugation with cellulose paper.

The ability of the two fusions to capture IgG antibodies was tested next. Tests were performed by dispensing a specific amount of each fusion onto the control and test zones of a µPAD. Following washing with buffer, a solution of an IgG antibody labelled with FITC was ran through the µPAD, incubated, washed with buffer again, incubated and analysed on a microscope for fluorescent signals. Antibody capture by either fusion should result in a fluorescent signal over the area where the molecules were spotted.

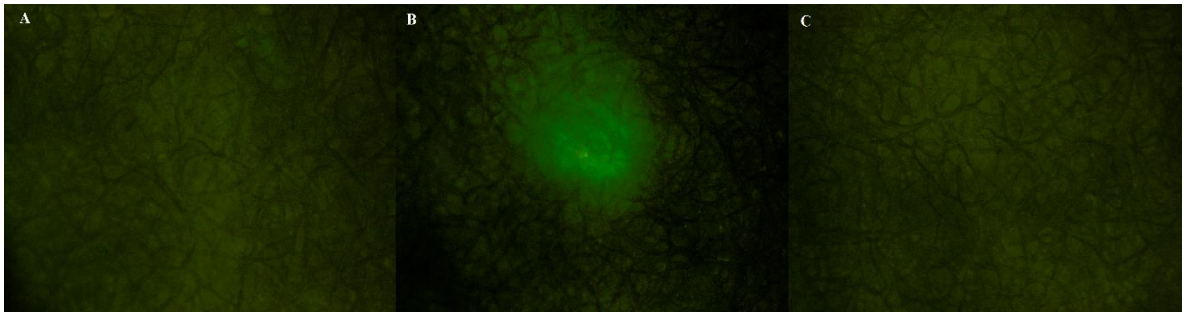

Figure 17 – Testing of the affinity of ZZ-CBM$_{64}$ and ZZapo-CBM$_{64}$ fusions towards IgG antibodies. Tests were performed by dispensing specific amounts of each fusion on distinct locations within a µPAD channel. A solution of an IgG antibody labelled with FITC was ran through the µPAD and test zones were imaged by fluorescence microscopy. A) Blanc (no molecules spotted); B) ZZ-CBM$_{64}$ was spotted before incubation; C) ZZapo-CBM$_{64}$ was spotted before incubation.

Figure 17 represents the snapshots of µPAD zones where ZZ-CBM$_{64}$ (Figure 17-B) and ZZapo-CBM$_{64}$ (Figure 17-C) were added. A control zone was also imaged (Figure 17-A). The results show that the ZZ-CBM$_{64}$ fusion successfully captured the labelled IgG

antibodies as expected, as judged by the brighter fluorescence spot on the matrix, where the fusion was dispensed (Figure 17-B). On the contrary, no fluorescence signal was detected at the site where the ZZapo-CBM_{64} was dispensed (Figure 17-C). This confirms that the ZZapo affibody is not able to recognize IgG antibodies as expected, as it was designed to specifically bind to Apo-A1.

8.4 PREPARATION OF µPAD TESTS

Three main designs of lateral flow tests were made and tested to determine the optimal flow of sample and the optimal volume of liquid necessary to spot the control and test areas. These designs are represented on Figure 18.

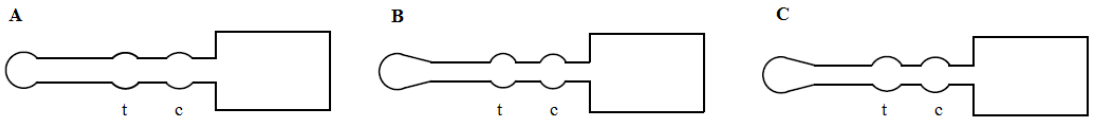

Figure 18 – Designs of the µPAD tests tested for optimization of sample flow and reagent spotting until the final obtained design (C).

The general design shows three areas to spot the samples and a reservoir for flow-through, the whole area of the test holds about 25 µL of volume at a time, however, additional washes can be made if a piece of paper is held on top of the flow-through area, as it will adsorb the excess buffer. Control (c) and test (t) areas hold 0.5 µL of liquid at a time, additional volumes can be added 0.5 µL at a time after the previous spot has dried completely. This is necessary to limit the distribution of molecules to the desired area. The first area is to introduce the sample into the µPAD. The first design (Figure 18-A) showed a very rapid flow rate, which can be problematic since the c and t areas are less time exposed to the sample, and the c and t areas were not well defined after melting, causing spotted molecules to flow out of the desired area. On the second design (Figure 18-B) the channel reduced in width, shower a better flow rate, and more defined c and t areas, however after melting they became too small to hold the desired volume for spotting. The area to spot the sample was also re-designed to allow faster adsorption and to facilitate the flow. The final design (Figure 18-C) had adjustments made to the c and t areas to hold the desired volume of spotted molecules.

These paper devices should not be placed in direct contact with a bench surface when running a test to prevent the migrating liquids to wet the surface. Rather, the device should be suspended to allow liquid to hang freely beneath the paper surface. This effect can be

observed in the control and test zones shown in Figure 19. However, if the devices are not suspended in such a way as to guarantee a perfectly horizontal surface, the liquid may take a longer time to migrate across the channels. Having the test being run on a flat surface could make it more reliable and easy. With this in mind, an adhesive membrane was applied to the bottom of the test paper strips, opposite to the side where the channel was printed, to enable the running of tests on a flat surface. A number of experiments tests were then made to determine the influence of the adhesive membrane in the migrating velocity of fluids through the µPAD, as well as any other unexpected effects that could occur.

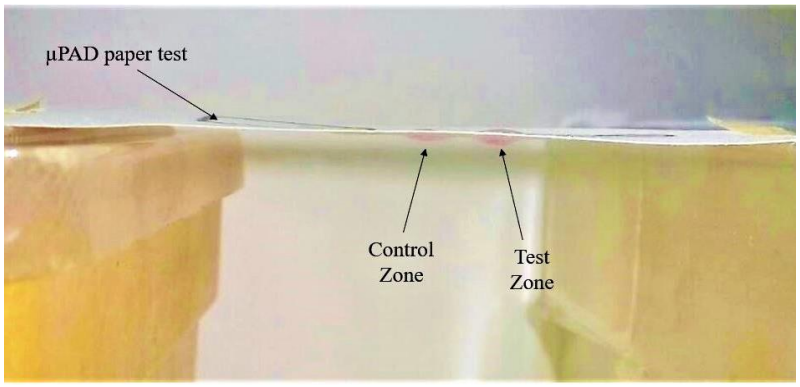

Figure 19 – Lateral view of a suspended µPAD test. Liquid drops are seen hanging below the paper strip in the control and test zones.

In the first set of experiments conducted, a sample containing food dye diluted in running buffer was run through two µPADs, one with an adhesive membrane beneath and another suspended (Figure 20-A). An observation of the devices shows that the dye migrated through the channels with velocity inferior to the velocity of the liquid (Figure 20-A). Nevertheless, the liquid front was still visible and allowed the recording of the migration distance as a function of time (Figure 20-B). The results show that liquids running in µPADs using a bottom adhesive layer moved considerably faster than in those without adhesive. According to the Washburn's equation, which describes capillary flow, the time t required for a liquid of dynamic viscosity η and surface tension γ to penetrate a distance L in the channel, is proportional to the square of L, where D is the pore Diameter:

$$t = \frac{4\eta}{\gamma D} L^2$$

From the linearization of this equation (Figure 20-B) we can further confirm that the tests using the adhesive membrane have higher slopes than those without the membrane, translating into a higher velocity of flow.

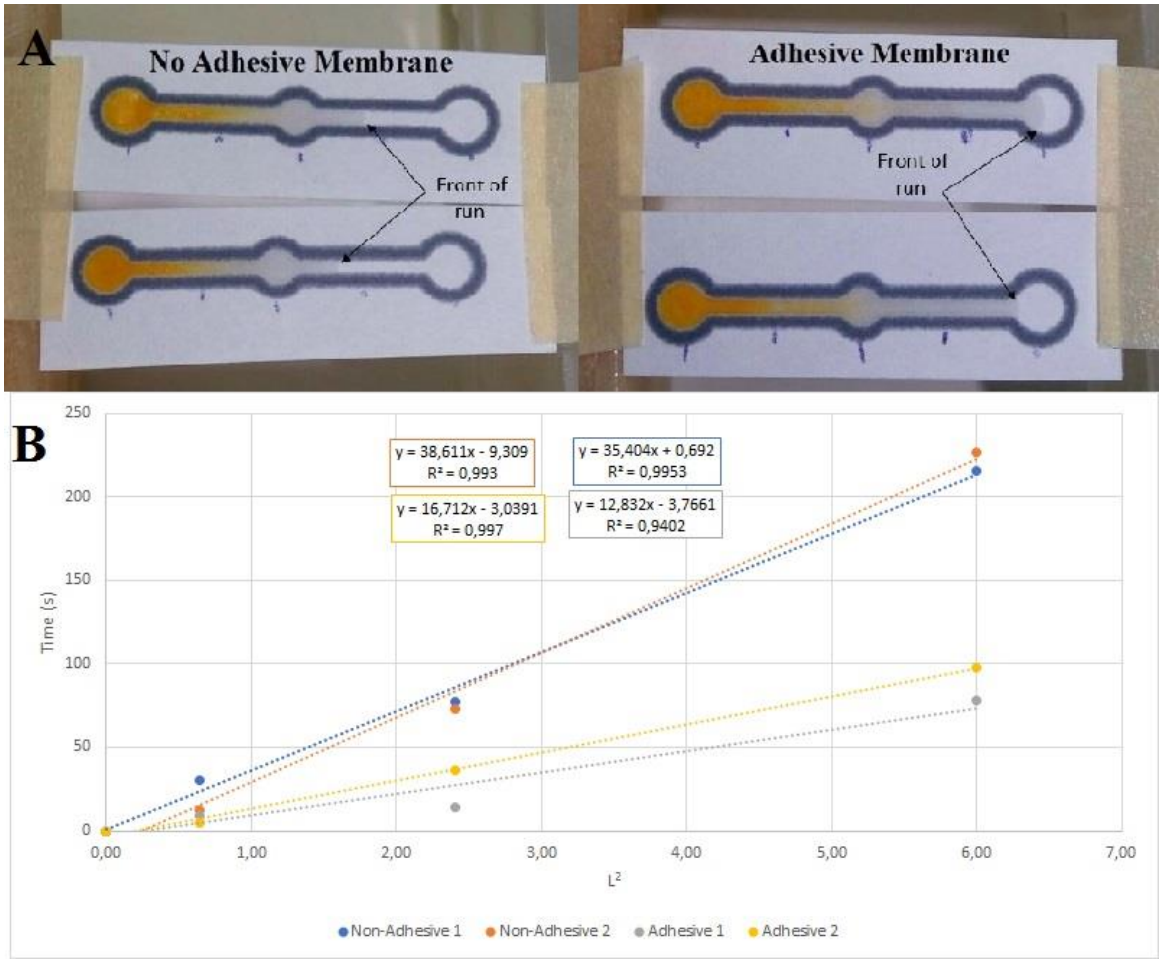

Figure 20 – A) Sample velocity tests of a mixture of food coloring and PBS buffer in µPADs with and without an adhesive membrane. B) Linearization of Washburn's equation using the times of the front of the run vs the distance marked on the paper strips with blue dots.

In a second set of experiments, the migration of plain AuNPs and of AuNPs conjugated with the anti-Apo-A1 antibody was compared in µPADs without and with adhesive membrane. From this point forward, unless stated otherwise, all tests were run with 5pmol of Ab-Goat in the control area and 5pmol of ZZapo-CBM_{64} diluted in running buffer to a total volume of 1 µL in the test area. The first tests showed that the migration of conjugated AuNPs was hampered in both µPADs with and without adhesive membrane due to unspecific binding to the cellulose microfibrils (Figure 21-A1, B1). To remove this unwanted binding, the surfactant Tween 20, which is a blocker commonly used to remove non-specific binding, was added to the buffer at a concentration of 0.05% (v/v).

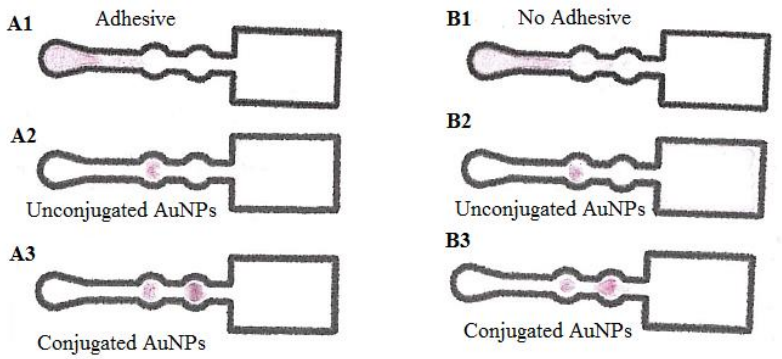

Figure 21 - µPADs with (A1, A2, A3) and without (B1, B2, B3) adhesive membrane on the bottom, ran with ZZapo-CBM_{64} in the test zone and Goat anti-mouse antibody in the control zones, with samples containing: A1) Conjugated AuNPs diluted in PBS buffer; B1) Conjugated AuNPs diluted in PBS buffer; A2) Unconjugated AuNPs diluted in PBS buffer with 0.05% Tween20; B2) Unconjugated AuNPs diluted in PBS buffer with 0.05% Tween20; A3) Conjugated AuNPs diluted in PBS buffer with 0.05% Tween20; B3) Conjugated AuNPs diluted in PBS buffer with 0.05% Tween20.

As shown in Figure 21-A2, A3, B2 and B3, after the addition of Tween 20 in the buffer, the AuNPs flowed through the channel and did not bind to the cellulose before reaching the test zones. Furthermore, the use of the adhesive membrane did not have any noticeable impact on the migration across the test strips (Figure 21-A2, A3). Thus, µPADs with adhesive on the bottom were used in all subsequent tests. As expected, the AuNPs conjugated with the mouse Anti-Apo-A1 antibody were captured at the control site by the pre-deposited anti-mouse goat antibody, as judged by the presence of a red spot on the control zone of the µPADs (Figure 21-A3, B3). However, non-specific binding between ZZapo-CBM_{64} in the test zone with conjugated AuNPs (Figure 21-A3, B3) was detected. A similar result was obtained when running unconjugated AuNPs (Figure 21-A2, B2), which indicates that the non-specific binding is due to a nanoparticle-ZZapo-CBM_{64} interaction, and not due to the Anti-Apo-A1 antibody. One way to address this problem would be to change the composition of buffer used in the tests. The first option was to increase the concentration of Tween 20. However, high concentrations of Tween 20 could not be used because the surfactant tends to permeabilize the wax walls. To assess at which concentration this happens, tests were made in circular areas bounded by wax circumferences using a dye solubilized in buffers with concentrations of Tween 20 ranging from 0.05-0.25% (v/v). 15 µL of these solutions were dispensed over the circular areas 5µL at a time, with drying in between. The results in Figure 22 show that concentrations of Tween 20 higher than 0.15% will cause leakage of fluids through the wax walls, and thus cannot be used in running buffers.

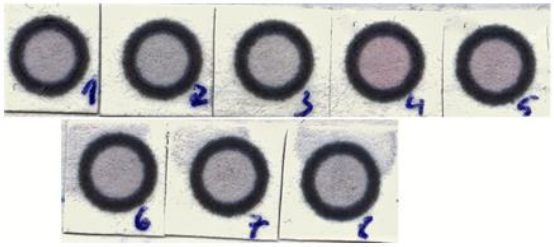

Figure 22 – Spot assays of a dye solution mixed with PBS buffer with varying concentrations of Tween20: 1) 0.05% Tween20; 2) 0.08% Tween20; 3) 0.1% Tween20; 4) 0.12% Tween20; 5) 0.15% Tween20; 6) 0.17% Tween20; 7) 0.2% Tween20; 8) 0.25% Tween20.

Experiments were then performed with buffers with Tween 20 concentrations lower than 0.15% to see if they removed the unwanted binding. µPADs were ran with conjugated AuNPs diluted in running buffer and ran through the LFA, washing the channel twice with the same buffer. From the results shown in Figure 23-b to Figure 23-f we can observe that the increased concentration of Tween 20 did not remove the unwanted non-specific binding at the used concentrations, so another approach must be used.

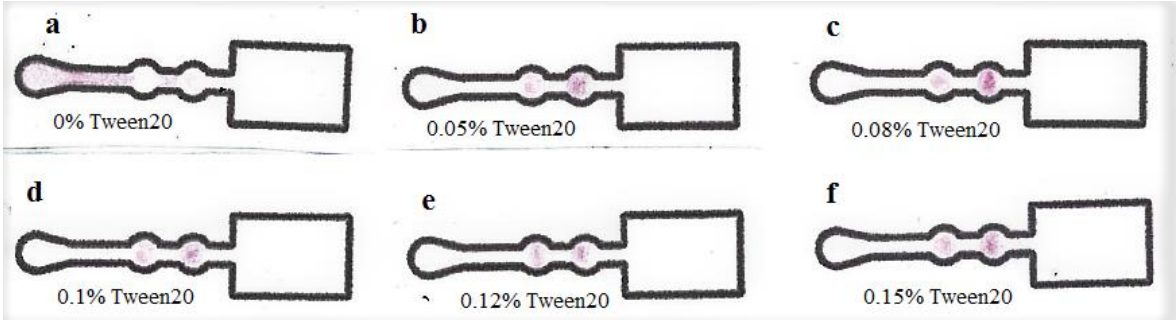

Figure 23 - µPADs with adhesive membrane ran with ZZapo-CBM_{64} in the test zone and Goat anti-mouse antibody in the control zones, the sample ran contained Anti-Apo-A1 conjugated AuNPs diluted in PBS buffer with varying concentrations of Tween20.

Bovine Serum Albumin (BSA) is another commonly used protein blocker in protein assays, and it was used in the running buffer at a concentration of 0.1% (w/v), along with 0.08% Tween 20. A few different methodologies were used to evaluate the most efficient way of removing the non-specific interactions. The resulting tests are shown in Figure 24. In Figure 24-A the test was run in the same way as the previous ones, but the washing step and dilution of conjugated AuNPs was done using the new buffer containing BSA. Figure 24-B shows a similar test but with an additional pre-washing step with the new buffer, after dispensing the ZZapo-CBM_{64} and goat anti-mouse antibody in the test and control areas, respectively, and before running the sample through the test. The example in Figure 24-C, ZZapo-CBM_{64} was incubated in the new buffer for 5min before spotting it into the test area, and then run in the same way as shown in Figure 24-A. In the example shown in Figure 24-

D, we used BSA conjugated AuNPs, where 100µL of conjugated AuNPs were incubated with 100µL of a 0.1% BSA solution for 20min, centrifuged and the pellet was resuspended in the buffers used for AuNP functionalization to a final volume of 100µL. The test was run in the same conditions as the first one. Tests shown in Figure 24-E and 24-F were done using the same methodology as in the ones shown in Figure 24-C and 24-D respectively, but with the additional pre-washing step used in the case of the test of Figure 24-B. From the resulting tests, we can see that a combination of pre-washing the channels with AuNPs conjugated with BSA or ZZapo-CBM_{64} conjugated with BSA were the only methodologies that efficiently eliminated the non-specific capture of AuNPs by ZZapo-CBM_{64}. The other tests (Figure 24-A-D) all showed a positive signal in the test zone, although it was considerably less intense than when using a running buffer without BSA, as it blocks binding sites of the molecules creating competitive binding. The running buffer to be used from this point forward is PBS, 0.08% Tween 20 and 0.1% BSA, as well as BSA conjugated AuNPs, which can be conjugated in a batch, and the µPAD channels will be pre-washed with this buffer before running a sample.

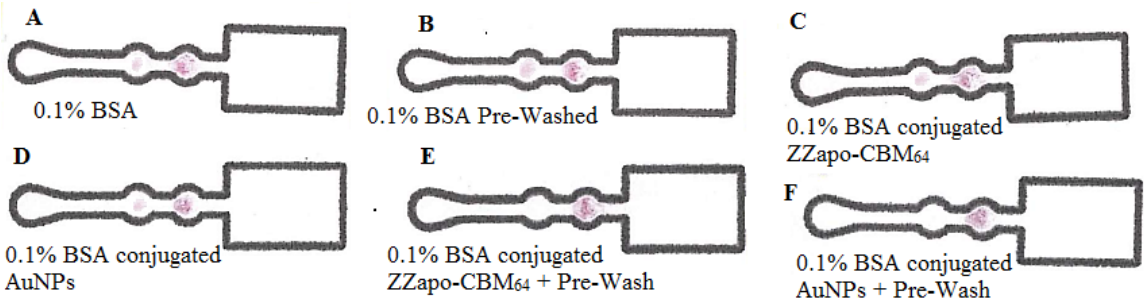

Figure 24 - µPADs ran with ZZapo-CBM_{64} in the test zone and Ab-Goat in the control zones, the sample ran contained Anti-Apo-A1 conjugated AuNPs diluted in PBS buffer with 0.1% BSA and 0.08% Tween20. A) the buffer was used in the sample dilution; B) The channel was pre-washed with the buffer before adding the sample; C) ZZapo-CBM_{64} was incubated with the buffer before spotting the test zone; D) BSA conjugated AuNPs were used in the sample; E) ZZapo-CBM_{64} was incubated with the buffer before spotting the test zone and the channel was pre-washed with the buffer; F) BSA conjugated AuNPs were used in the sample and the channel was pre-washed with the buffer.

8.5 CAPTURE AND DETECTION OF APOLIPOPROTEIN-A1

µPAD tests with and without adhesive membrane were conducted to evaluate the capture and detection of Apo-A1 by ZZapo-CBM_{64} and Anti Apo-A1 and BSA conjugated AuNPs (Figure 25). AuNPs were incubated with Apo-A1 and running buffer for 10min, while ZZapo-CBM_{64} and control antibody were spotted into the test and control areas of the µPAD, using the buffer to pre-wash the channel once the spots were dried. The ratio of Apo-A1 to ZZapo-CBM_{64} was 2:1, to assure enough Apo-A1 reached the test zone.

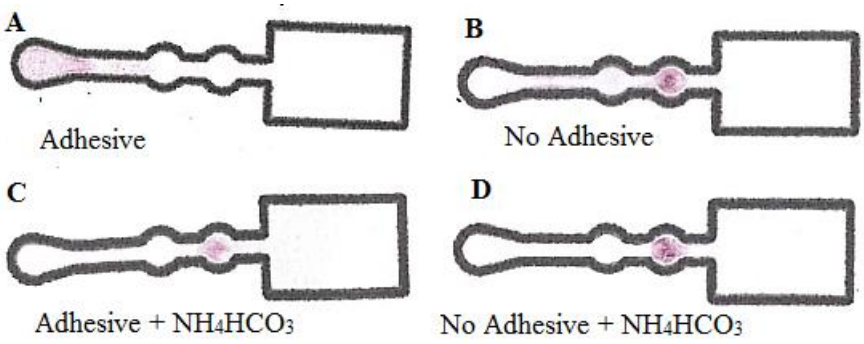

Figure 25 - µPADs ran with ZZapo-CBM$_{64}$ in the test zone and Ab-Goat in the control zones, the sample ran contained Anti-Apo-A1 and BSA conjugated AuNPs and Apo-A1, diluted in: A) PBS buffer with 0.1% BSA and 0.08% Tween20, using an adhesive membrane on the bottom of the paper strip; B) PBS buffer with 0.1% BSA and 0.08% Tween20, without the adhesive membrane on the bottom of the paper strip; : C) NH_4HCO_3 10mM buffer with 0.1% BSA and 0.08% Tween20, using an adhesive membrane on the bottom of the paper strip; D) NH_4HCO_3 10mM buffer with 0.1% BSA and 0.08% Tween20, without the adhesive membrane on the bottom of the paper strip.

From the tests we can see that Apo-A1 does not seem to be captured in the test zone by ZZapo-CBM$_{64}$, as there is no noticeable signal (Figure 25). Furthermore, the use of the adhesive membrane caused some interaction with Apo-A1 holding the sample in the channel before reaching the test zone, as shown by the AuNPs in this area (Figure 25-A-B). This effect was not as significant in suspended tests without the adhesive membrane and could be eliminated with a change of running buffer. This was tested by using the buffer NH_4HCO_3 (10mM, pH 7.4), as it was the buffer used by Sigma-Aldrich in the purified Apo-A1, with 0.08% Tween20 and 0.1% BSA (Figure 25-C-D). The use of this new buffer completely removed the retention of the sample in the initial part of the test in both µPADs with and without the adhesive membrane. Apo-A1 detection was not accomplished in either case, which could mean that the ZZapo-CBM64 construct is not capturing Apo-A1 as intended.

To determine if Apo-A1 capture is not occurring, two methodologies were used. First, samples of these molecules were incubated and ran through a Basic Native-PAGE. Several gels were run with different conditions (mainly with different voltages, running time and buffer pH), and the best resulting gel is presented in Figure 26. Lanes 1, 2 and 3 represent ZZapo-CBM$_{64}$, Apo-A1 and Anti-Apo-A1 respectively. Lane 5 represents a mixture of ZZapo-CBM$_{64}$ and Apo-A1, lane 7 is a mixture of Apo-A1 and Anti-Apo-A1, lane 9 represents a mixture of all three molecules and lanes 4, 6, 8 and 10 were loaded with loading buffer to maintain the same density in all lanes, some bands can be observed from leakage from other wells. Although the results are not highly conclusive, they provide some insight into the interactions between the molecules. In lane 5 we can clearly see the band corresponding to ZZapo-CBM$_{64}$ between two other less visible bands representing Apo-A1.

If these molecules interacted, a different band would be visible representing the complex. Since this was not the case, the ZZapo-CBM_{64} construct was likely not capturing Apo-A1. In lane 7 we can clearly see the bands that correspond to Anti-Apo-A1, however the bands for Apo-A1 are not visible, which indicates that Anti-Apo-A1 was successfully capturing Apo-A1. In this case a different migration pattern is not expected since the antibody is very large and does not migrate far into the gel. Finally, in lane 9 bands representing ZZapo-CBM_{64} and Anti-Apo-A1 are visible, but not the one for Apo-A1, indicating that the intended complex of the three molecules was not formed likely due to ZZapo-CBM_{64} being unable to capture Apo-A1.

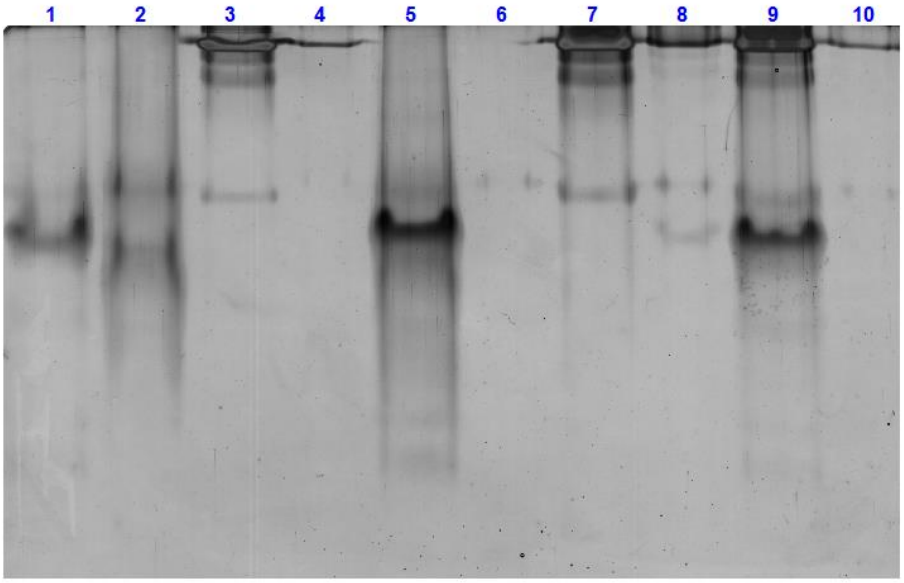

Figure 26 – Testing of the affinity ZZapo-CBM_{64} fusion towards Apo-A1, as well as Anti-Apo-A1 antibody affinity to Apo-A1. The mixtures were incubated, loading buffer was added and the mixtures were then analysed by Native-PAGE. Lanes: 1) ZZapo-CBM_{64}; 2) Apo-A1; 3) Anti-Apo-A1; 5) Mixture of ZZapo-CBM_{64} and Apo-A1; 7) Mixture of Apo-A1 and Anti-Apo-A1; 9) Mixture of ZZapo-CBM_{64}, Apo-A1 and Anti-Apo-A1.

To further validate the results observed in the Native PAGE, a cellulose binding test was done by incubating samples of ZZapo-CBM_{64}, Apo-A1 and Anti-Apo-A1 antibody with cellulose microparticles, centrifuging and running the supernatant through SDS-PAGE (Figure 27). If any protein binds to ZZapo-CBM_{64}, then the complex will sink to the bottom along with the cellulose particles and not be present in the supernatant. All mixtures were done in 1:1 ratios and diluted equally.

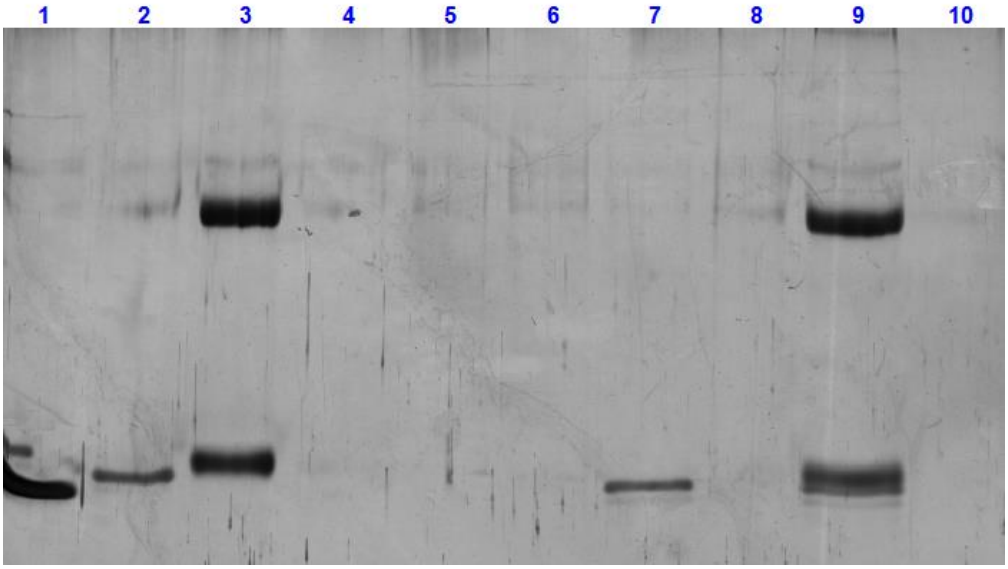

Figure 27 - Silver Stained SDS-PAGE of cellulose affinity test using ZZapo-CBM$_{64}$ of: 1) ZZapo-CBM$_{64}$; 2) Apo-A1; 3) Anti-Apo-A1; 5) Supernatant of ZZapo-CBM$_{64}$ incubation and centrifugation with cellulose particles; 7) Supernantant of the incubation and centrifugation of the mixture of Apo-A1 and ZZapo-CBM$_{64}$ with cellulose particle; 9) Supernantant of the incubation and centrifugation of the mixture of Apo-A1, Anti-Apo-A1 and ZZapo-CBM$_{64}$ with cellulose particles.

Lane 1 corresponds to ZZapo-CBM$_{64}$ which looks deformed because the gel was slightly malformed, while Lane 2 was attributed to Apo-A1, and Lane 3 to Anti-Apo-A1 antibody, all diluted in PBS buffer. Lanes 4, 6, 8 and 10 were loaded with diluted running buffer, to avoid density differences between lanes. Lane 5 represents ZZapo-CBM$_{64}$ after incubation with cellulose nanoparticles, the lack of signal meaning it successfully bound to the particles, as expected. Lane 7 represents a mixture of ZZapo-CBM$_{64}$ and Apo-A1 after the incubation with cellulose, resulting in a band corresponding to Apo-A1, which means that in these conditions, ZZapo-CBM$_{64}$ is not capturing Apo-A1 as intended. Lane 9 represents a mixture of all molecules after incubation with cellulose, resulting in three bands, the first two corresponding to Anti-Apo-A1, and the last one representing Apo-A1. From these results we can conclude that the ZZapo-CBM$_{64}$ complex is not capturing Apo-A1. There also should be no interaction between Anti-Apo-A1 and ZZapo-CBM$_{64}$ since the band remains after the incubation with cellulose. Another cellulose binding experiment was done where the mixtures were incubated in different pH buffers and with different times to assess if different incubation conditions could promote Apo-A1 capture by ZZapo-CBM$_{64}$, the resulting gels are presented in Figure 28.

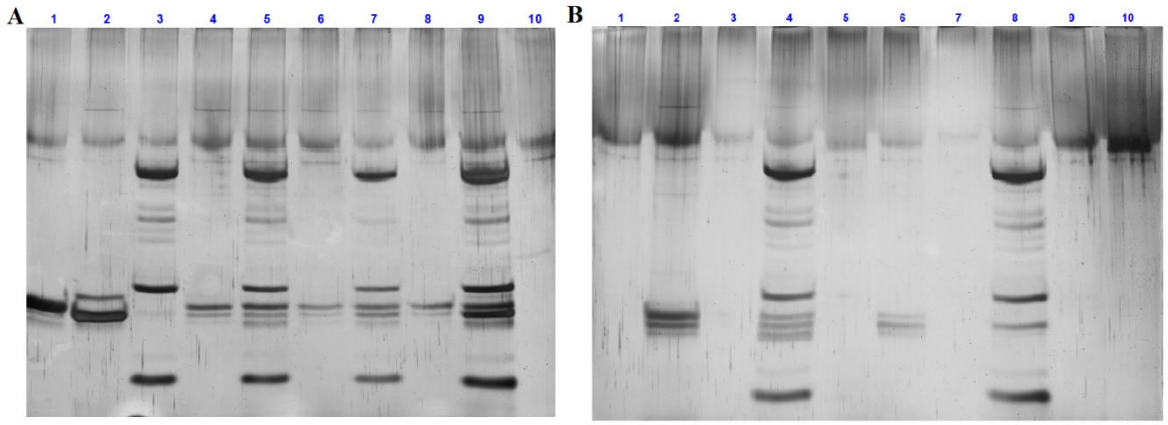

Figure 28 - Silver Stained SDS-PAGE of cellulose affinity test using ZZapo-CBM$_{64}$ of: A-1) Apo-A1; A-2) ZZapo-CBM$_{64}$; A-3) Anti-Apo-A1; A-4) Mixture of ZZapo-CBM$_{64}$ and Apo-A1 in PBS pH 7.6; A-5) Mixture of ZZapo-CBM$_{64}$, Apo-A1 and Anti-Apo-A1 in PBS pH 7.6; A-6) Mixture of ZZapo-CBM$_{64}$ and Apo-A1 in PBS pH 8.6; A-7) Mixture of ZZapo-CBM$_{64}$, Apo-A1 and Anti-Apo-A1 in PBS pH 8.6; A-8) Mixture of ZZapo-CBM$_{64}$ and Apo-A1 in PBS pH 9.6; A-9) Mixture of ZZapo-CBM64, Apo-A1 and Anti-Apo-A1 in PBS pH 9.6; B-2) Mixture of ZZapo-CBM$_{64}$ and Apo-A1 in PBS pH 7.6 incubated overnight; B-4) Mixture of ZZapo-CBM$_{64}$, Apo-A1 and Anti-Apo-A1 in PBS pH 7.6 incubated overnight; B-6) Mixture of ZZapo-CBM$_{64}$ and Apo-A1 in PBS pH 7.6 incubated for 2h; B-8) Mixture of ZZapo-CBM$_{64}$, Apo-A1 and Anti-Apo-A1 in PBS pH 7.6 incubated for 2h.

Lane A-1 represents Apo-A1, lane A-2 represents ZZapo-CBM$_{64}$, lane A-3 represents Anti-Apo-A1. In all the lanes of both gels, more bands appeared than what was expected, one band for A-1 and A-2 and two bands for A-3. This effect has been previously studied by other authors (118), and are most likely fragments resulting from the sample preparation process for SDS-PAGE. These authors found that longer incubation at 100ºC times and high concentrations of DTT can cause fragmentation and the addition of an alkylating agent, such as iodoacetamide or N-ethylmaleimide, could reduce this effect. The experiment was not repeated with these alkylating agents due to limited sample size of Apo-A1 and Anti-Apo-A1. Lanes A-4, A-6 and A-8 represent mixtures of ZZapo-CBM$_{64}$ and Apo-A1 in PBS pH 7.6, 8.6 and 9.6 respectively, and lanes A-5, A-7 and A-9 represent mixtures of ZZapo-CBM$_{64}$, Apo-A1 and Anti-Apo-A1 in PBS pH 7.6, 8.6 and 9.6 respectively. Lanes B-2 and B-6 represent mixtures of ZZapo-CBM$_{64}$ and Apo-A1 in PBS pH 7.6 incubated overnight and for 2h respectively, and lanes B-4 and B-8 represent mixtures of ZZapo-CBM$_{64}$, Apo-A1 and Anti-Apo-A1 in PBS pH 7.6 incubated overnight and for 2h respectively. From this experiment we can conclude that no matter the incubation conditions, the capture of Apo-A1 by ZZapo-CBM$_{64}$ was not achieved since in all cases Apo-A1 is present in the supernatant after the incubation with ZZapo-CBM$_{64}$ and cellulose particles. As expected there was also no interaction between ZZapo-CBM$_{64}$ and Anti-Apo-A1, since the antibody is present in all cases and did not bind to ZZapo-CBM$_{64}$ or the cellulose particles.

To discover the reason why ZZapo-CBM_{64} is not capturing Apo-A1, further studies should be made. One hypothesis is that the 3D structure of the construct could be folded in such a way that covers the part that recognizes and binds Apo-A1, making it unable to interact with the affibody, however this hypothesis could not be tested.

9 CONCLUSION

Antibodies are the main affinity molecule of choice for biochemical immunological applications, due to the extensive knowledge already available. These molecules, however present some limitations due to their molecular structure. As such, recent efforts have been made to discover new affinity molecules with simpler structures and high affinities. Affibodies are one of these novel affinity proteins, and have already been applied in several fields such as imaging, diagnostics, therapies, bioassays and biosensors. Furthermore, affibodies are also a great alternative to antibodies due to simpler and cheaper synthetization methods, as well as showing versatility, not only in immunoassays, but also in imaging, therapeutics, protein purification and other bioassays. Affibodies can target several molecules, such as Apo-A1 which has been discovered to be involved in several immunomodulatory effects, and further understanding of these technologies could provide novel advances in therapeutics and diagnostics.

POC testing has come to revolutionize molecular testing, since it has the potential of delivering diagnostic results rapidly, while also being simple, inexpensive, disposable and portable, so it is vital that these technologies are further developed for implementation. POC technologies include microfluidic devices such as µPADs, which present exceptional versatility due to their capacity of being composed of different materials, involving different kinds of detection and fabrication methods, as well as flexible and extremely customizable designs to suit whatever necessity the user needs, as reviewed in many works throughout this paper. These tests are made up of paper matrixes with hydrophobic barriers as the test medium, which considerably reduces prices, is easily disposable and portable, amounting to an exceptional device in resource limited setting.

As such, the main objective of this work was to develop and optimize a simple µPAD test for a capture assay using a custom made affibody molecule connected to a CBM (ZZapo-CBM_{64}) that could bind to the paper matrix of the µPAD and capture a target of interest, in this case Apo-A1 was used as a model, and successfully achieve detection using AuNPs conjugated with an Anti-Apo-A1 antibody.

In this work, ZZapo-CBM_{64} was successfully produced and purified. To investigate if the purified ZZapo-CBM_{64} had the correct sequence, purified plasmid DNA was sequenced and compared with the original ZZapo-CBM_{64} sequence, which did not yield any mismatches, thus, the plasmid was correctly produced. Several tests were done to compare

it with ZZ-CBM_{64}, a similar construct used to capture IgG rather than just Apo-A1. Both presented similar binding properties to cellulose, provided by the CBM_{64} part of the construct, successfully binding to cellulose particles and chromatography paper in a solution. Furthermore, capture capacity of IgG was assessed using IgG labelled with FITC for fluorescent analysis. ZZ-CBM_{64} captured IgG labelled to FITC successfully while the new ZZapo-CBM_{64} did not.

A µPAD test was successfully designed and optimized for sample flow and reagent spotting using the AutoCad program. The use of an adhesive membrane on the bottom of the test strips also encouraged a faster elution of the sample and allowed the test to be run on a flat surface, as opposed to suspended.

Anti-Apo-A1 conjugated and unconjugated AuNPs were ran through paper tests which got stuck in the initial part of the channel, but by adding Tween20 to the running buffer this problem was no longer observable. ZZapo-CBM_{64} showed a false positive signal when Apo-A1 was not present, due to unspecific binding, which was solved by adding BSA to the running buffer and washing the channels with the same buffer before adding the sample. Additionally, this membrane did not show any other effects with Anti-Apo-A1 conjugated and unconjugated AuNPs. If the sample contained Apo-A1 the adhesive membrane had some interaction with it, causing the sample to not flow through the test, but by using a NH_4HCO_3 buffer instead of PBS, this problem was solved.

Detection of Apo-A1 in the µPAD tests was not achieved. Native-PAGE and a cellulose binding test were conducted to ascertain the cause of the failed capture. Results indicated that ZZapo-CBM_{64} was not capturing Apo-A1, being the cause for not having a successful detection.

Future works could include the study of the 3D structure of ZZapo-CBM_{64}, in order to understand if it has any influence in the capture zone and if it could be the reason Apo-A1 is not being captured. Furthermore, other affibody variants could be studied to understand if the problem observed is a common factor in constructs such as the one presented in this work or not. Once this is accomplished, optimization of the detection system should be made, working with detection limits to develop a test that if positive or negative detects an anomaly in the test subjects' organism (i.e. low Apo-A1 levels could indicate chronic liver or kidney disease, if the tests' detection range is at normal levels, a negative result could mean an

anomaly). The following steps could be testing in actual blood samples for validation of the method.

BIBLIOGRAPHY

1. Areosa F, Cardoso E, Pacheco F. Fundamentos de Imunologia. Lidel; 2012.

2. Löfblom J, Feldwisch J, Tolmachev V, Carlsson J, Ståhl S, Frejd FY. Affibody molecules : Engineered proteins for therapeutic , diagnostic and biotechnological applications. FEBS Lett. 2010;584(12):2670–80.

3. Nygren PÅ. Alternative binding proteins: Affibody binding proteins developed from a small three-helix bundle scaffold. FEBS J. 2008;275(11):2668–76.

4. Nord Karin, Gunneriusson E, Ringdahl J, Ståhl S, Uhlén M NP. Binding proteins selected from combinatorial libraries of an alpha- helical bacterial receptor domain. Nat Biotechnol. 1997;15(8):772–7.

5. Andersson M, Rönnmark J, Areström I, Nygren PÅ, Ahlborg N. Inclusion of a non-immunoglobulin binding protein in two-site ELISA for quantification of human serum proteins without interference by heterophilic serum antibodies. J Immunol Methods. 2003;283(1–2):225–34.

6. Mouratou B. Artificial Affinity Proteins as Ligands of Immunoglobulins. Biomolecules. 2015;1(5):60–75.

7. Malm M, Bass T, Gudmundsdotter L, Lord M, Frejd F, Stahl S, Lofblom J. Engineering of a bispecific affibody molecule towards HER2 and HER3 by addition of an albumin-binding domain allows for affinity purification and in vivo half-life extension. Biotechology J. 2014;9(9):1215–22.

8. Lindgren J, Ekblad C, Abrahmsøn L, Eriksson A. A Native Chemical Ligation Approach for Combinatorial Assembly of Affibody Molecules. 2012;1024–31.

9. Justino CIL, Duarte AC, Rocha-Santos TAP. Analytical applications of affibodies. TrAC - Trends Anal Chem. 2015;65:73–82.

10. Baum RP, Prasad V, Dirk M, Schuchardt C, Orlova A, Wennborg A, Tolmachev V, Feldwisch J. Molecular Imaging of HER2 -Expressing Malignant Tumors in Breast Cancer Patients Affibody Molecules. 2015;51(6):892–8.

11. Orlova A, Wållberg H, Stone-Elander S, Tolmachev V. On the Selection of a Tracer for PET Imaging of HER2-Expressing Tumors : Direct Comparison of a 124 I-Labeled Affibody Molecule and Trastuzumab in a Murine Xenograft Model. J Nucl Med. 2009;50:417–25.

12. Ahlgren S, Orlova A, Wållberg H, Hansson M, Sandström M, Lewsley R, Abrahmsén L, Tolmachev V, Feldwisch J, Hansson M, Sandstr M, Lewsley R. Targeting of HER2-Expressing Tumors Using 111In-ABY-025, a Second-Generation Affibody Molecule with a Fundamentally Reengineered Scaffold. J Nucl Med. 2010;51:1131–8.

13. Ahlgren S, Wallberg H, Tran TA, Widstrom C, Hjertman M, Abrahmsén L, Berndorff D, Dinkelborg LM, Cyr JE, Feldwisch J, Orlova A, Tolmachev V. Targeting of HER2-Expressing Tumors with a Site-Specifically 99mTc-Labeled Recombinant Affibody Molecule, ZHER2:2395, with C-Terminally Engineered Cysteine. 2009;781–9.

14. Altai M, Wallberg H, Orlova A, Rosested M, Hosseinime SJ, Tolmachev V, Stahl S. Order of amino acids in C-terminal cysteine-containing peptide-based chelators influences cellular processing and biodistribution of 99m Tc-labeled recombinant Affibody molecules. Amino Acids. 2012;1975–85.

15. Malmberg J, Sandström M, Wester K, Tolmachev V, Orlova A. Comparative biodistribution of imaging agents for in vivo molecular profiling of disseminated prostate cancer in mice bearing prostate cancer xenografts : focus on 111 In- and 125 I-labeled anti-HER2 humanized monoclonal trastuzumab and ABY-025 Affibody. Nucl Med Biol. 2011;38(8):1093–102.

16. Rosik D, Thibblin A, Antoni G, Honarvar H, Strand J, Selvaraju RK, Altai M, Orlova A, Eriksson A, Tolmachev V. Incorporation of a Triglutamyl Spacer Improves the Biodistribution of Synthetic A ffi body Molecules Radio fl uorinated at the N - Terminus via Oxime Formation with 18 F - 4-

Fluorobenzaldehyde. Bioconjug Chem. 2014;25(1):82–92.

17. Gao J, Chen K, Miao Z, Ren G, Chen X, Gambhir SS, Cheng Z. Affibody-based nanoprobes for HER2-expressing cell and tumor imaging. Biomaterials. 2011;32(8):2141–8.

18. Yang M, Cheng K, Qi S, Liu H, Jiang Y, Jiang H, Li J, Chen K. Affibody modified and radiolabeled gold-Iron oxide hetero-nanostructures for tumor PET, optical and MR imaging. Biomaterials. 2013;34(11):2796–806.

19. Sörensen J, Sandberg D, Sandström M, Wennborg A, Feldwisch J, Tolmachev V, Åström G, Lubberink M, Garske-román U, Carlsson J, Lindman H, Lubberink M, Garske-rom U, Carlsson J, Lindman H. Cancer Metastases Using the 111 In-ABY-025 Affibody Molecule. 2014;730–5.

20. Justino CIL, Freitas AC, Pereira R, Duarte AC, Rocha Santos TAP. Recent developments in recognition elements for chemical sensors and biosensors. TrAC - Trends Anal Chem. 2015;68:2–17.

21. Tolmachev V, Orlova A, Pehrson R, Galli J, Baastrup B, Andersson K, Sandstro M, Rosik D, Lundqvist H, Wennborg A, Nilsson FY. Radionuclide Therapy of HER2-Positive Microxenografts Using a Lu-Labeled HER2-Specific Affibody Molecule. Cancer Res. 2007;67(6):2773–82.

22. Wållberg H, Löfdahl P-åke, Tschapalda K, Uhlén M, Tolmachev V, Nygren P-åke, Ståhl S. Affinity recovery of eight HER2-binding affibody variants using an anti-idiotypic affibody molecule as capture ligand. Protein Expr Prep. 2011;76:127–35.

23. Andersson C, Hansson M, Power U. Mammalian cell production of a respiratory syncytial virus (RSV) candidate vaccine recovered using a product-specific affinity column. Biotechmol Appl Biochem. 2001;32:25–32.

24. Lee H, Weng Y, Ku W, Huang LLH. A nanobead based sandwich immunoassay. J Taiwan Inst Chem Eng. 2012;43(1):9–14.

25. Hennig C, Rink L, Fagin U, Jabs WJ, Kirchner H. The influence of naturally occurring heterophilic anti-immunoglobulin antibodies on direct measurement of serum proteins using sandwich ELISAs. J Immunol Methods. 2000;235(1–2):71–80.

26. Thermofisher Scientific [Internet]. Overview of ELISA. [cited 2017 Jan 2]. Available from: https://www.thermofisher.com/pt/en/home/life-science/protein-biology/protein-biology-learning-center/protein-biology-resource-library/pierce-protein-methods/overview-elisa.html

27. Oda MN, Budamagunta MS, Borja MS, Petrlova J, Voss JC, Lagerstedt JO. The secondary structure of apolipoprotein A-I on 9 . 6-nm reconstituted high-density lipoprotein determined by EPR spectroscopy. FEBS J. 2013;280(14):3416–24.

28. Curtiss LK, Valenta DT, Hime NJ, Rye K, Curtiss LK, Valenta DT, Hime NJ, Rye K. What Is So Special About Apolipoprotein AI in Reverse Cholesterol Transport ? Arter Thromb Vasc Biol. 2006;26(1):12–9.

29. Huang Y, Didonato JA, Levison BS, et al. An abundant dysfunctional apolipoprotein A1 in human atheroma. Nat Med. 2014;20(2):193–203.

30. Schaefer EJ, Anthanont P, Diffenderfer MR, Polisecki E, Asztalos BF. Diagnosis and treatment of high density lipoprotein deficiency. Prog Cardiovasc Dis. 2016;

31. Luo J, Wärmländer SKTS, Gräslund A, Abrahams JP. Cross interactions between the Alzheimer ' s disease amyloid-β peptide and other amyloid proteins : a further aspect of the amyloid cascade hypothesis. Biol Chem. 2016;291(32):16485–93.

32. Lewis TL, Cao D, Lu H, Mans RA, Su YR, Jungbauer L, Linton MF, Fazio S, Lu H, Li L. Overexpression of Human Apolipoprotein A-I Preserves Cognitive Function and Attenuates Neuroinflammation and Cerebral Amyloid Angiopathy in a Mouse Model of Alzheimer. Biol Chem. 2010;285(47):36958–68.

33. Gordon SM, Hofmann S, Askew DS, Davidson WS. High density lipoprotein : it's not just about lipid

transport anymore. Trends Endocrinol Metab. 2011;22(1):9–15.

34. Zamanian-daryoush M, Lindner D, Tallant TC, Wang Z, Buffa J, Klipfell E, Parker Y, Hatala D, Parsons-wingerter P, Rayman P, Yusufishaq MSS, Fisher EA, Smith JD, Finke J, Didonato JA, Hazen SL. The Cardioprotective Protein Apolipoprotein A1 Promotes Potent Anti-tumorigenic Effects. Biol Chem. 2013;288(29):21237–52.

35. Li H, Wang D, Zhang H, Kirmani K, Zhao Z, Steinmetz R, Xu Y. Lysophosphatidic acid stimulates cell migration , invasion , and colony formation as well as tumorigenesis / metastasis of mouse ovarian cancer in immunocompetent mice. Mol Cancer Ther. 2009;8(6):1692–701.

36. Kozel TR, Burnham-Marusich AR. Point-of-Care Testing for Infectious Diseases: Past, Present, and Future. J Clin Microbiol. 2017;55(8):2313–20.

37. St John A, Price CP. Existing and Emerging Technologies for Point-of-Care Testing. Clin Biochem Rev. 2014;35(3):155–67.

38. Mabey D, Peeling RW, Ustianowski A, Perkins MD. Tropical infectious diseases: Diagnostics for the developing world. Nat Rev Microbiol. 2004;2(3):231–40.

39. Ehrmeyer SS, Laessig RH. Point-of-care testing, medical error, and patient safety: A 2007 assessment. Clin Chem Lab Med. 2007;45(6):766–73.

40. Gu W, Kim Y, Geun B, Demirci U, Khademhosseini A. Nano/Microfluidics for diagnosis of infectious diseases in developing countries. Adv Drug Deliv Rev. 2010;62(4–5):449–57.

41. Bissonnette L, Bergeron MG. Diagnosing infections — current and anticipated technologies for point-of-care diagnostics and home-based testing. Eur Soc Clin Infect Dis. 2010;16(8):1044–53.

42. Hawkins K, Weigl B. Microfluidic diagnostics for low-resource settings. Proc Spie. 2010;7593:75930L–1–15.

43. Erickson KA, Wilding P. Evaluation of a novel point-of-care system, the i-STAT Portable Clinical Analyzer. Clin Chem. 1993;39(2):283–7.

44. Yager P, Domingo GJ, Gerdes J. Point-of-Care Diagnostics for Global Health. Annu Rev Biomed Eng. 2008;10(1):107–44.

45. Posthuma-Trumpie GA, Korf J, Van Amerongen A. Lateral flow (immuno)assay: Its strengths, weaknesses, opportunities and threats. A literature survey. Anal Bioanal Chem. 2009;393(2):569–82.

46. Salomone A, Mongelli M, Roggero P, Boscia D. Reliability of Detection of Cistrus Tristeza Virus by an Immunochromatographic Lateral Flow Assay in Comparison with ELISA. 2004;86:43–8.

47. Nielsen K, Yu WL, Lin M, Davis SAN, Elmgren C. Prototype Single Step Lateral Flow Technology for Detection of Avian Influenza Virus and Chicken Antibody to Avian Influenza Virus. J Immunoass Immunochem. 2007;(28):37–41.

48. Carrio A, Sampedro C, Sanchez-Lopez JL, Pimienta M, Campoy P. Automated Low-Cost Smartphone-Based Lateral Flow Saliva Test Reader for Drugs-of-Abuse Detection. Sensors (Basel). 2015 Nov 24;15(11):29569–93.

49. Nilghaz A, Wicaksono DHB, Gustiono D, Abdul Majid FA, Supriyanto E, Abdul Kadir MR. Flexible microfluidic cloth-based analytical devices using a low-cost wax patterning technique. Lab Chip. 2012;12(1):209.

50. Osborn JL, Lutz B, Fu E, et al. Microfluidics without pumps: reinventing the T-sensor and H-filter in paper networks. Lab Chip. 2010;10(20):2659.

51. Lisowski P, Zarzycki PK. Microfluidic paper-based analytical devices (μPADs) and micro total analysis systems (μTAS): Development, applications and future trends. Chromatographia. 2013;76(19–20):1201–14.

52. Hu J, Wang S, Wang L, Li F, Pingguan-Murphy B, Lu TJ, Xu F. Advances in paper-based point-of-

care diagnostics. Biosens Bioelectron. 2014;54:585–97.

53. Muller RH, Clegg ANDDL, York N. Automatic Paper Chromatography. Ann N Y Acad Sci. 1951;1123–5.

54. Martinez AW, Phillips ST, Butte MJ, Whitesides GM. Patterned paper as a platform for inexpensive, low-volume, portable bioassays. Angew Chemie - Int Ed. 2007;46(8):1318–20.

55. Yetisen AK, Akram MS, Lowe CR. Paper-based microfluidic point-of-care diagnostic devices. Lab Chip. 2013;13(12):2210–51.

56. Pelton R. Bioactive paper provides a low-cost platform for diagnostics. TrAC - Trends Anal Chem. 2009;28(8):925–42.

57. Martinez, A. W.; Phillips, S. T.; Whitesides GM. Diagnostics for the Developing World : Microfluidic Paper-Based Analytical Devices. Anal Chem. 2010;82(1):3–10.

58. Yamada K, Shibata H, Suzuki K, Citterio D. Toward practical application of paper-based microfluidics for medical diagnostics: state-of-the-art and challenges. Lab Chip. 2017;(7).

59. Li X, Ballerini DR, Shen W. A perspective on paper-based microfluidics: Current status and future trends. Biomicrofluidics. 2012;6(1).

60. Yang Y, Noviana E, Nguyen MP, Geiss BJ, Dandy DS, Henry CS. Paper-Based Microfluidic Devices : Emerging Themes and Applications. Anal Chem. 2016;(88):71–91.

61. Jahanshahi-anbuhi S, Pennings K, Leung V, Kannan B, Brennan JD, Filipe CDM, Pelton RH. Design Rules for Fluorocarbon-Free Omniphobic Solvent Barriers in Paper-Based Devices. Appl Mater interfaces. 2015;7:25434–40.

62. Xu C, Cai L, Zhong M, Zheng S. Low-cost and rapid prototyping of microfluidic paper-based analytical devices by inkjet printing of permanent marker ink. RSC Adv. 2014;5:4770–3.

63. Mitchell HT, Noxon IC, Chaplan CA, Carlton SJ, Liu CH, Ganaja KA, Martinez NW, Immoos CE, Costanzo PJ, Martinez AW. Reagent pencils: a new technique for solvent-free deposition of reagents onto paper-based microfluidic devices. Lab Chip. 2015;17–20.

64. Oyola-reynoso S, Heim AP, Halbertsma-black J, Zhao C, Tevis ID, Simge Ç, Cademartiri R, Liu X, Bloch J, Thuo MM. Draw your assay : Fabrication of low-cost paper-based diagnostic and multi-well test zones by drawing on a paper. 2015;145:73–7.

65. Carrilho E, Martinez AW, Whitesides GM. Wax Printing – a Simple Micropatterning Process for Paper-based Microfluidics. Anal Chem. 2009;81(16):1–5.

66. Songjaroen T, Dungchai W, Chailapakul O, Laiwattanapaisal W. Novel, simple and low-cost alternative method for fabrication of paper-based microfluidics by wax dipping. Talanta. 2011;85(5):2587–93.

67. Lu R, Shi W, Jiang L, Qin J, Lin B. Rapid prototyping of paper-based microfluidics with wax for low-cost, portable bioassay. Electrophoresis. 2009;30(9):1497–500.

68. Kavruk M, Ozalp VC, Oktem AH. Portable Bioactive Paper-Based Sensor for Quantification of Pesticides. J Anal Methods Chem. 2013;2013:8.

69. Rosa AMM, Louro AF, Martins SAM, Inácio J, Azevedo AM, Prazeres DMF. Capture and detection of DNA hybrids on paper via the anchoring of antibodies with fusions of carbohydrate binding modules and ZZ-domains. Anal Chem. 2014;86(9):4340–7.

70. Nery EW, Kubota LT. Evaluation of enzyme immobilization methods for paper-based devices—A glucose oxidase study. J Pharm Biomed Anal. 2015;(117):551–9.

71. Brash JL, Ten Hove P. Protein adsorption studies on “standard” polymeric materials. J Biomater Sci Polym Ed. 1993;4(6):591–9.

72. Halder E, Chattoraj DK, Das KP. Adsorption of biopolymers at hydrophilic cellulose-water interface. Biopolymers. 2005;77(5):286–95.

73. Wang J, Pelton R, Veldhuis LJ, MacKenzie Cr, Hall Jc, Filipe CD. Wet-strength Resins and Surface Properties Affect Paper-based Antibody Assays. Appita J J Tech Assoc Aust New Zeal Pulp Pap Ind. 2010;63(1):32.

74. Su S, Ali MM, Filipe CDM, Li Y, Pelton R. Microgel-based inks for paper-supported biosensing applications. Biomacromolecules. 2008;9(3):935–41.

75. Kong F, Hu YF. Biomolecule immobilization techniques for bioactive paper fabrication. Anal Bioanal Chem. 2012;403(1):7–13.

76. Su S, Nutiu R, Filipe CDM, Li Y, Pelton R. Adsorption and covalent coupling of ATP-binding DNA aptamers onto cellulose. Langmuir. 2007;23(3):1300–2.

77. Bora U, Sharma P, Kannan K, Nahar P. Photoreactive cellulose membrane-A novel matrix for covalent immobilization of biomolecules. J Biotechnol. 2006;126(2):220–9.

78. Tiller JC, Rieseler R, Berlin P, Klemm D. Stabilization of activity of oxidoreductases by their immobilization onto special functionalized glass and novel aminocellulose film using different coupling reagents. Biomacromolecules. 2002;3(5):1021–9.

79. Kawaguchi H, Fujimoto K, Mizuhara Y. Hydrogel microspheres III. Temperature-dependent adsorption of proteins on poly-N-isopropylacrylamide hydrogel microspheres. Colloid Polym Sci. 1992;270(1):53–7.

80. Shoseyov O, Shani Z, Levy I. Carbohydrate Binding Modules: Biochemical Properties and Novel Applications. Microbiol Mol Biol Rev. 2006;70(2):283–95.

81. Hussack G, Luo Y, Veldhuis L, Hall JC, Tanha J, MacKenzie R. Multivalent anchoring and oriented display of single-domain antibodies on cellulose. Sensors. 2009;9(7):5351–67.

82. Ofir K, Berdichevsky Y, Benhar I, Azriel-Rosenfeld R, Lamed R, Barak Y, Bayer EA, Morag E. Versatile protein microarray based on carbohydrate-binding modules. Proteomics. 2005;5(7):1806–14.

83. Tolba M, Brovko LY, Minikh O, Griffiths MW. Engineering of bacteriophages displaying affinity tags on its head for biosensor applications. NSTI Nanotech. 2008;2:449–52.

84. Cate DM, Adkins JA, Mettakoonpitak J, Henry CS. Recent developments in paper-based microfluidic devices. Anal Chem. 2015;87(1):19–41.

85. Karita S, Kaneta T. Chelate titrations of Ca2+ and Mg2+ using microfluidic paper-based analytical devices. Anal Chim Acta. 2016;924:60–7.

86. Cate DM, Noblitt SD, Volckens J, Herny CS. Multiplexed Paper Analytical Device for Quantification of Metals using Distance-Based Detection David. Lab Chip. 2015;(15):2808–18.

87. Abe K, Suzuki K, Citterio D. Inkjet-printed microfluidic multianalyte chemical sensing paper. Anal Chem. 2008;80(18):6928–34.

88. Yang X, Forouzan O, Brown TP, Shevkoplyas SS. Integrated separation of blood plasma from whole blood for microfluidic paper-based analytical devices. Lab Chip. 2012;12(2):274–80.

89. Ge S, Ge L, Yan M, Song X, Yu J, Huang J. A disposable paper-based electrochemical sensor with an addressable electrode array for cancer screening. Chem Commun. 2012;48(75):9397–9.

90. Nie Z, Nijhuis CA, Gong J, Chen X, Kumachev A, Martinez AW, Narovlyansky M, Whitesides GM. Electrochemical sensing in paper-based microfluidic devices. Lab Chip. 2010;10(4):477–83.

91. Dungchai W, Chailapakul O, Henry CS. Electrochemical detection for paper-based microfluidics. 2009;81(14):5821–6.

92. Li L, Kong Q, Zhang Y, Dong C, Ge S, Yu J. A 3D electrochemical immunodevice based on a porous

Pt-paper electrode and metal ion functionalized flower-like Au nanoparticles. J Mater Chem B. 2015;3:2764–9.

93. Yang J, Nam Y, Lee S, Kim C, Koo Y, Chang W, Gunasekaran S. Paper-fluidic electrochemical biosensing platform with enzyme paper and enzymeless electrodes. Sensors Actuators B Chem. 2014;203:44–53.

94. Li Z, Li F, Wee HW, Han LY, Pingguan-Murphy B, Lu TJ, Xu F. Direct writing electrodes using ball pen for paper-based point-of-care testing. Analyst. 2015;16:5526–35.

95. Syedmoradi L, Daneshpour M, Alvandipour M, Gomez FA, Hajghassem H, Omidfar K. Point of care testing: The impact of nanotechnology. Biosens Bioelectron. 2017;87:373–87.

96. Zhao W, Ali MM, Aguirre SD, Brook MA, Li Y. Paper-based bioassays using gold nanoparticle colorimetric probes. Anal Chem. 2008;80(22):8431–7.

97. Cordeiro M, Carlos FF, Pedrosa P, Lopez A, Baptista PV. Gold Nanoparticles for Diagnostics : Advances towards Points of Care. 2016;(i).

98. Xianyu Y, Wang Z, Jiang X. Plasmonic ELISA for the ultrasensitive detection of disease biomarkers with the naked eye. ACS Nano. 2014;12(8):12741–7.

99. Rica R De, Stevens MM. Plasmonic ELISA for the ultrasensitive detection of disease biomarkers with the naked eye. Nat Nanotechnol. 2012;12(7):821–4.

100. Kumar A, Hens A, Arun RK, Chatterjee M, Mahato K, Layek K, Chanda N. A paper based microfluidic device for easy detection of uric acid using positively charged gold nanoparticles. Analyst. 2015;4(8):1166–9.

101. Saleh M, Soliman H, Haenen O, El-Matbouli M. Antibody-coated gold nanoparticles immunoassay for direct detection of Aeromonas salmonicida in fish tissues. J Fish Dis. 2011;34(11):845–52.

102. Anfossi L, Baggiani C, Giovannoli C, Giraudi G. Homogeneous immunoassay based on gold nanoparticles and visible absorption detection. Anal Bioanal Chem. 2009;394(2):507–12.

103. Sharma S, Zapatero-Rodríguez J, Estrela P, O'Kennedy R. Point-of-Care diagnostics in low resource settings: Present status and future role of microfluidics. Biosensors. 2015;5(3):577–601.

104. Lee S, Oncescu V, Mancuso M, Mehta S, Erickson D. A smartphone platform for the quantification of vitamin D levels. Lab Chip. 2014 Apr 21;14(8):1437–42.

105. Dou M, Sanjay ST, Benhabib M, Xu F, Li X. Low-cost bioanalysis on paper-based and its hybrid microfluidic platforms. Talanta. 2015 Dec 1;145:43–54.

106. Wang C, Hennek JW, Ainla A, Kumar AA, Lan W, Im J, Smith BS, Zhao M, Whitesides GM. A Paper-Based "Pop-up" Electrochemical Device for Analysis of Beta- Hydroxybutyrate. Anal Chem. 2016;88(12):6326–33.

107. Camplisson CK, Schilling KM, Pedrotti WL, Stone HA, Martinez AW. Two-ply channels for faster wicking in paper- based microfluidic devices. Lab Chip. 2015;15(23):4461–6.

108. Noiphung J, Songjaroen T, Dungchai W, Henry CS, Chailapakul O, Laiwattanapaisal W. Electrochemical detection of glucose from whole blood using paper-based microfluidic devices. Anal Chim Acta. 2013 Jul 25;788:39–45.

109. Wu Y, Xue P, Kang Y, Hui KM. Paper-Based Microfluidic Electrochemical Immunodevice Integrated with Nanobioprobes onto Graphene Film for Ultrasensitive Multiplexed Detection of Cancer Biomarkers. Anal Chem. 2013 Sep 17;85(18):8661–8.

110. Li X, Zhao C, Liu X, et al. A paper-based microfluidic biosensor integrating zinc oxide nanowires for electrochemical glucose detection. Microsystems Nanoeng. 2015 Aug 3;1:15014.

111. Zhou W, Gao X, Liu D, Chen X. Gold Nanoparticles for In Vitro Diagnostics. Chem Rev. 2015 Oct 14;115(19):10575–636.

112. Zhang L, Cao X, Wang L, Zhao X, Zhang S, Wang P. Printed microwells with highly stable thin-film enzyme coatings for point-of- care multiplex bioassay of blood samples Liting. Analyst. 2015;140:4105–13.

113. Nosrati R, Gong MM, Gabriel MCS, Pedraza CE. Paper-Based Quantification of Male Fertility Potential. Clin Chem. 2016;62:458–65.

114. Li M, Cao R, Nilghaz A, Guan L, Zhang X, Shen W. "Periodic-Table-Style" Paper Device for Monitoring Heavy Metals in Water. Anal Biochem. 2015;(87):2555–9.

115. Apilux A, Isarankura-na-ayudhya C, Tantimongcolwat T. Paper-based acetylcholinesterase inhibition assay combining a wet system for organophosphate and carbamate pesticides detection. Exp Clin Sci. 2015;(14):307–19.

116. Luo L, Li X, Crooks RM. Low-Voltage Origami-Paper-Based Electrophoretic Device for Rapid Protein Separation. Anal Chem. 2014;86:12390–7.

117. Pires MRV, Pereira PMM, Brás LAJ, Bule P, Cardoso V, Correia M, Alves VD, Najmudin S, Venditto I, Ferreira MAL, Romão MJ, Carvalho AL, Fontes CMGA, Prazeres DM. Stability and ligand promiscuity of type A carbohydrate-binding modules are illustrated by the structure of Spirochaeta thermophila StCBM64C. Biol Chem. 2017;12(292):4847–60.

118. Zhu ZC, Chen Y, Ackerman MS, Wang B, Wu W, Li B, Obenauer-kutner L, Zhao R, Tao L, Ihnat PM, Liu J, Gandhi RB, Qiu B. Investigation of monoclonal antibody fragmentation artifacts in non-reducing SDS-PAGE. J Pharm Biomed Anal. 2013;83:89–95.

APPENDIX A: MAP OF THE FINAL PET21A VECTOR

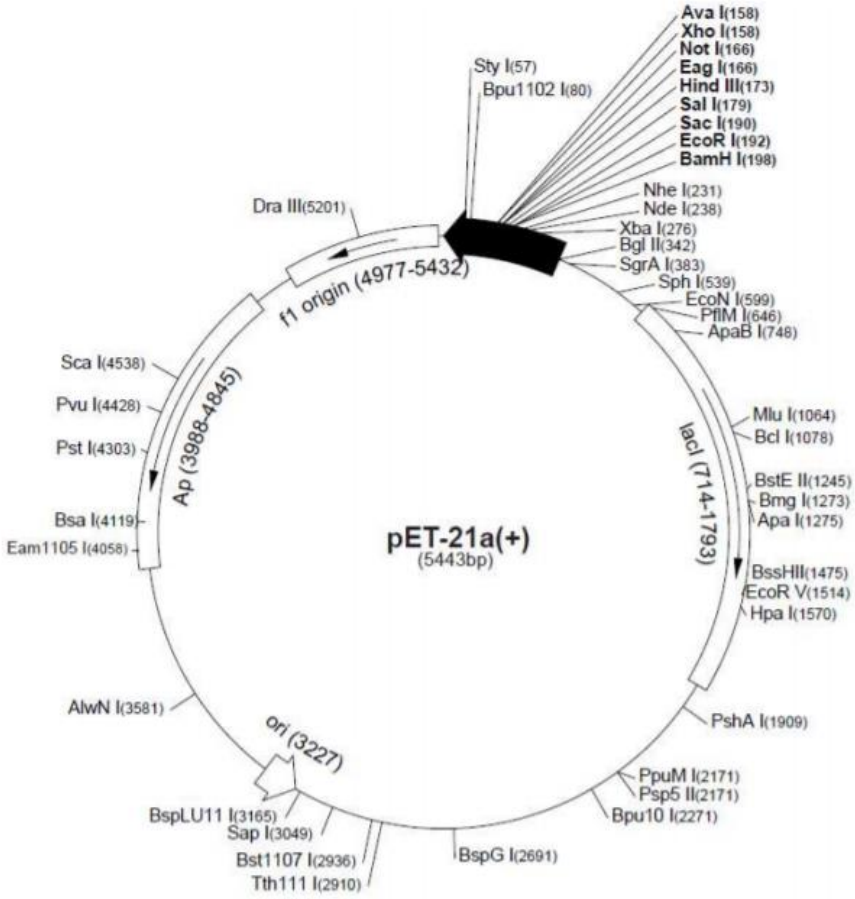

Figure 29 – Plasmid map of the final vector of pET21a containing the ZZapo-CBM$_{64}$ module and restriction enzymes marked on the vector.